Am J Physiol Heart Circ Physiol 319: H1459–H1473, 2020.
First published October 16, 2020; doi:10.1152/ajpheart.00247.2020.

RESEARCH ARTICLE | *Translational Physiology*

Estrogen receptor-α prevents right ventricular diastolic dysfunction and fibrosis in female rats

Tik-Chee Cheng,[1] Jennifer L. Philip,[2] Diana M. Tabima,[1] Santosh Kumari,[3,4] Bakhtiyor Yakubov,[5] Andrea L. Frump,[5] Timothy A. Hacker,[6] Alessandro Bellofiore,[7] Rongbo Li,[8] Xin Sun,[8] Kara N. Goss,[3,4] Tim Lahm,[5,9,10] and Naomi C. Chesler[1,4]

[1]*Department of Biomedical Engineering, University of Wisconsin-Madison, Madison, Wisconsin;* [2]*Department of Surgery, University of Wisconsin-Madison, Madison, Wisconsin;* [3]*Division of Allergy, Pulmonary and Critical Care Medicine, University of Wisconsin-Madison, Madison, Wisconsin;* [4]*Department of Medicine, University of Wisconsin-Madison, Madison, Wisconsin;* [5]*Division of Pulmonary, Critical Care, Sleep and Occupational Medicine, Department of Medicine, Indiana University School of Medicine, Indianapolis, Indiana;* [6]*Cardiovascular Research Center, University of Wisconsin-Madison, Madison, Wisconsin;* [7]*Department of Biomedical, Chemical and Materials Engineering, San Jose State University, San Jose, California;* [8]*Department of Pediatrics, University of California San Diego, La Jolla, California;* [9]*Department of Cellular and Anatomy, Cell Biology and Physiology, Indiana University School of Medicine, Indianapolis, Indiana; and* [10]*Richard L. Roudebush Veterans Affairs Medical Center, Indianapolis, Indiana*

Submitted 13 April 2020; accepted in final form 9 October 2020

Cheng TC, Philip JL, Tabima DM, Kumari S, Yakubov B, Frump AL, Hacker TA, Bellofiore A, Li R, Sun X, Goss KN, Lahm T, Chesler NC. Estrogen receptor-α prevents right ventricular diastolic dysfunction and fibrosis in female rats. *Am J Physiol Heart Circ Physiol* 319: H1459–H1473, 2020. First published October 16, 2020; doi:10.1152/ajpheart.00247.2020.—Although women are more susceptible to pulmonary arterial hypertension (PAH) than men, their right ventricular (RV) function is better preserved. Estrogen receptor-α (ERα) has been identified as a likely mediator for estrogen protection in the RV. However, the role of ERα in preserving RV function and remodeling during pressure overload remains poorly understood. We hypothesized that loss of functional ERα removes female protection from adverse remodeling and is permissive for the development of a maladapted RV phenotype. Male and female rats with a loss-of-function mutation in ERα (ERαMut) and wild-type (WT) littermates underwent RV pressure overload by pulmonary artery banding (PAB). At 10 wk post-PAB, WT and ERαMut demonstrated RV hypertrophy. Analysis of RV pressure waveforms demonstrated RV-pulmonary vascular uncoupling and diastolic dysfunction in female, but not male, ERαMut PAB rats. Similarly, female, but not male, ERαMut exhibited increased RV fibrosis, comprised primarily of thick collagen fibers. There was an increased protein expression ratio of TIMP metallopeptidase inhibitor 1 (Timp1) to matrix metalloproteinase 9 (Mmp9) in female ERαMut compared with WT PAB rats, suggesting less collagen degradation. RNA-sequencing in female WT and ERαMut RV revealed kallikrein-related peptidase 10 (Klk10) and Jun Proto-Oncogene (Jun) as possible mediators of female RV protection during PAB. In summary, ERα in females is protective against RV-pulmonary vascular uncoupling, diastolic dysfunction, and fibrosis in response to pressure overload. ERα appears to be dispensable for RV adaptation in males. ERα may be a mediator of superior RV adaptation in female patients with PAH.

NEW & NOTEWORTHY Using a novel loss-of-function mutation in estrogen receptor-α (ERα), we demonstrate that female, but not male, ERα mutant rats display right ventricular (RV)-vascular uncoupling, diastolic dysfunction, and fibrosis following pressure overload, indicating a sex-dependent role of ERα in protecting against adverse RV remodeling. TIMP metallopeptidase inhibitor 1 (Timp1), matrix metalloproteinase 9 (Mmp9), kallikrein-related peptidase 10 (*Klk10*), and Jun Proto-Oncogene (*Jun*) were identified as potential mediators in ERα-regulated pathways in RV pressure overload.

adverse remodeling; estrogen receptor-α; pressure overload; right ventricle

INTRODUCTION

Pulmonary arterial hypertension (PAH) is a disease characterized by progressive narrowing and stiffening of pulmonary arteries leading to increased right ventricular (RV) afterload. PAH has a prevalence of 6.6 to 26.0 cases per million adults with an incidence at 1.1 to 7.6 million adults annually (4). In response to the increased afterload, the RV initially hypertrophies and increases its contractility as an adaptive response to maintain coupling of the RV-pulmonary vascular circuit (65). With time, progressive afterload causes maladaptive RV remodeling with cardiac fibrosis (45), diastolic dysfunction (45), and uncoupling of the RV-pulmonary circuit (59). Without effective intervention, these processes lead to RV failure and increased mortality (65). The drivers and markers of the transition from adaptive to maladaptive RV remodeling are an area of intense research interest, which may be aided by greater understanding of the features of adaptive RV remodeling.

Despite the greater incidence of PAH in women (54), RV function is better preserved in women with PAH than in men (18). This suggests that the transition from adaptive to maladaptive remodeling may be sex-dependent. In estrogen-repleted ovariectomized female rats with sugen/hypoxia-induced pulmonary hypertension (SuHx-PH), increased RV expression of ERα, but not ERβ (15), suggests that ERα is the critical pathway for sex-dependent preservation of RV function in the context of pressure overload. In fact, in male SuHx-PH rats, treatment with ERα agonist 4,4′4′′[4-propyl-(1H)-pyrazole-1,3,5-triyl]

Correspondence: N. C. Chesler (nchesler@uci.edu).

tris-phenol (PPT) resulted in enhanced cardiac index and improved exercise capacity compared with untreated SuHx-PH rats, and ERα expression in female SuHx-PH rats correlated strongly and positively with cardiac output (CO) (15). Also, hypoxic pulmonary hypertensive male rats treated with the ERα antagonist methyl-piperidino-pyrazole showed a reversal of the beneficial effects of estrogen-mediated attenuation of RV hypertrophy and CO (26). These studies suggest a protective role of ERα in the RV of both females and males with experimental PH.

Evidence for a sex-based difference in ERα regulation in the left ventricle (LV) has been reported (10, 66). In an ischemia-reperfusion injury model, female ERα knockout (KO) mice exhibited significantly reduced myocardial function compared with female wild-type (WT) mice, whereas male ERα KO showed comparable function as male WT mice (66), implicating female cardiac protection through ERα. Furthermore, ERα binds to collagen types I and III promoters in female but not male rat cardiac fibroblasts, and collagen types I and III are downregulated following estrogen treatment in female but not male rat cardiac fibroblasts (10). However, it is unclear whether this sex bias in collagen regulation is also present in the RV. Moreover, although it is known that ERα regulates mitochondrial respiration and ultrastructure (47, 48, 74), a knowledge gap exists regarding ERα regulation of mitochondrial homeostasis in the pressure overloaded RV.

Although ERα signaling has been studied in the RV before, prior studies using SuHx (15, 26) or monocrotaline (61) to study the role of estrogen signaling in RV adaptation to PH have been confounded by interaction effects in the pulmonary vasculature. In particular, estrogen signaling in the context of SuHx-PH (15, 27) and monocrotaline-induced PH (61) confers protection against pulmonary vascular remodeling such that the stimulus for RV remodeling is decreased. In contrast, constriction of the main pulmonary artery by banding (PAB), especially when matched to the size of the animal (6), creates a robust increase in afterload that is not modified by estrogen signaling. We used this PAB model and a novel loss-of-function ERα rat model (14) to study the role of ERα during adaptive RV remodeling, characterized as preserved RV-pulmonary vascular coupling. We hypothesized that the loss of functional ERα during the adaptive stage of RV remodeling removes female protection from RV-pulmonary vascular uncoupling, RV diastolic dysfunction, and myocardial fibrosis.

MATERIALS AND METHODS

Animal studies. We used 38 male or female Sprague–Dawley rats (10–11 wk old) in this study. Eighteen rats had a targeted loss-of-function mutation of ERα (ERαMut) and 20 of littermates had the wild-type ERα (WT). Details of the generation of the loss-of-function ERα mutant rats via clustered regularly interspaced short palindromic repeats (CRISPR) have been reported in abstract form (14). All rats underwent baseline echocardiography, during which the pulmonary artery (PA) diameter was measured. Following echocardiography, rats were randomly assigned to PAB ($n = 5$ for each sex) or sham ($n = 4$–5 for each sex) surgery. The animal protocol was reviewed and approved by the University of Wisconsin Institutional Animal Care and Use Committee.

Pulmonary artery banding and sham surgery. PAB and sham surgeries were performed through a lateral thoracotomy and dissection of the main PA as described before (6). Briefly, rats were anesthetized with isoflurane (5% and then maintained at 2%–3%, balanced with oxygen), intubated, and ventilated. In PAB rats, a silk suture was tied around the main PA and a reference needle to achieve ~60% constriction based on the baseline echocardiographic diameter of the PA. In Sham rats, the suture was not tied. Rat bodyweight was collected weekly for up to 10 wk postoperatively.

Cardiac hemodynamics. At 10 wk postsurgery, rats were anesthetized with urethane (1.2 g/kg ip), intubated, and ventilated for right heart catheterization. Systemic pressure was measured at the aortic arch by advancing a pressure catheter (Millar, Houston, TX) through the right carotid artery. RV pressure was measured directly by a high fidelity catheter (Scisense, London, Ontario, Canada) inserted into the RV through the apex. Commercial software (Notocord Systems, Croissy Sur Seine, France) was used to record RV pressure waveforms at 1,000 Hz. RV end-systolic pressure (Pes) and RV maximal derivative of pressure (dP/dt_{max}) were derived from the RV pressure data. Ventricular vascular coupling (E_{es}/E_a) was calculated as: $E_{es}/E_a = (P_{iso}/\text{RV Pes})-1$, in which P_{iso} represents the maximum isovolumetric pressure. P_{iso} was estimated using a single beat method based on the second derivative of the pressure trace, as previously reported (3). Using the pressure waveforms, Tau Weiss (an indicator of diastolic function) was calculated using an exponential decay model as previously proposed (69) and modified as recommended elsewhere (28). Quality hemodynamic data were not collected in four rats, specifically in one female WT Sham, one male and one female WT PAB, and one female ERαMut Sham. Significant blood loss in two of the rats reduced systemic pressure, while difficulty with anesthesia prevented us from collecting hemodynamic data in the other two rats. All hemodynamic data analyses were performed by a blinded observer.

Serum collection and estrogen measurement. After euthanasia, ~1.5 mL of blood was collected, spun down at 4,000 rpm for 10 min at 4°C, aliquoted, and stored at −80°C. Serum samples were thawed on ice for estrogen measurement using Calbiotech Mouse/Rat Estradiol ELISA kit (Calbiotech, El Cajon, CA) according to manufacturer's instructions and as performed previously (15).

Gross evaluation. The RV free wall was separated from the left ventricle (LV) and septum and weighed. RV hypertrophy was calculated three different ways: *1*) RV weight scaled to tibia length (TL), *2*) RV weight scaled to terminal bodyweight (BW), and *3*) RV weight scaled to the sum of LV and septal weights (i.e., the Fulton index). The RV was then divided into five sections for the following analyses.

In situ mitochondrial oxidative consumption and analysis. A piece of RV tissue was placed in cold BIOPS solution, containing 10 mM Ca-EGTA, 0.1 μM free calcium, 20 mM imidazole, 20 mM taurine, 50 mM K-MES, 0.5 mM DTT, 6.56 mM $MgCl_2$, 5.77 mM ATP, and 15 mM phosphocreatine (pH 7.1), dissected to tease apart individual fibers into a mesh-like sample, and then permeabilized by gentle agitation in BIOPS with 5 mg/mL saponin (43). Permeabilized fibers were washed in MiR05 respiration media, containing 0.5 mM EGTA, 20 mM taurine, 3 mM $MgCl_2$, 110 mM sucrose, 60 mM K-lactobionate, 10 mM KH_2PO_4, 20 mM K-HEPES, and 1 mg/mL BSA (pH 7.1) and then placed in an Oxygraph-2k (Oroboros Instruments, Innsbruck, Austria) for oxygen flux measurement.

Oxygen flux data acquisition and analysis were performed using software DatLab (Oroboros Instruments, Austria) as previously reported (57). Respiration of permeabilized muscle fibers was measured in the Oxygraph-2k at 37°C with constant stirring. The same suite of substrates and inhibitors presented previously (25) was used here. Briefly, glutamate (10 mM) and malate (2 mM) were added as respiratory substrates (State 4 ADP-depleted basal respiration). Next, ADP (5 mM) was added to assess oxidative phosphorylation (OXPHOS) capacity (State 3 OXPHOS). Respiratory control ratio (RCR) was then calculated as State 3/State 4. The lack of a significant change in oxygen flux after adding cytochrome-*c* (10 μM) confirmed the integrity of the outer mitochondrial membrane (24). Complex II respiration was then assessed by inhibiting complex I with rotenone (1.25 mM) and stimulating complex II with succinate (10 mM). Complex IV respiration was measured by inhibiting both complex I and complex II with antimycin A (2.5 mM) and stimulating complex IV with a combination of *N,N,N′,*

N′-tetramethyl-*p*-phenylenediamine (TMPD) (0.5 mM) and ascorbate (2 mM). Oxygen flux was normalized to wet tissue weight as previously reported by (57).

Electron microscopy and mitochondrial ultrastructure image analysis. RV tissue cold-fixed in Karnovsky's fixative (Electron Microscopy Sciences, Hatfield, PA) was processed for transmission electron microscopy and mitochondrial ultrastructural image analysis as previously described (6). From a single RV tissue of a rat, five micrographs were captured at ×5,600 magnification and analyzed using ImageJ (1.49v; National Institutes of Health, Bethesda, MD). Mitochondria per high-power field are reported as the average number of mitochondria counted in five micrographs. Mitochondrial size is reported as average cross-sectional area of mitochondria in five micrographs as reported previously (6). These analyses were performed by a blinded observer.

Histology and image analysis. RV tissue was immersion fixed in 10% vol/vol buffered formalin (Thermo Fisher Scientific, Waltham, MA) and preserved in 70% ethanol. RV tissues were embedded in paraffin, sectioned, and stained with Picrosirius red to visualize collagen (6) or hematoxylin and eosin to visualize cardiomyocytes (67). To quantify total collagen deposition in the RV, the area containing collagen was determined by color thresholding in a representative field of view using MetaVue software (Optical Analysis Systems). To calculate percent collagen area, collagen area was divided by the tissue area in each field of view. Under polarized light, collagen organization and structure were determined. Collagen fibers are organized into tightly packed collagen bundles that appear as thick collagen fibers or diffusely distributed as thin collagen fibers (38). Both thick collagen fibers that impart properties of stiffness and thin collagen fibers that impart properties of elasticity contribute to diastolic function (19). Thick and thin collagen fibers were identified as areas of yellow/orange/red color or green color, respectively (5, 8, 22). The area of thick or thin collagen was divided by the total image area. The area of thick or thin collagen was calculated per image and then averaged to obtain a single measurement for each animal. RV cardiomyocyte cross-sectional area was measured by the cell area under the cross-sectional orientation. At least four representative fields of views were collected at ×20 magnification for each animal. All histological analyses were performed by a blinded observer.

RNA preparation and RNAseq analysis. Total RNA was extracted from 10 mg of RV using RNeasy Fibrous Tissue Mini Kit (Qiagen, Valencia, CA). DNase I treatment was performed in the column according to the manufacturer's protocol. 60 μL of total RNA was recovered with concentrations ranging from 72.7 to 180.6 ng/μL and with A260/280 nm ranging from 1.89 to 2.11. RNA samples were submitted to UW Madison Biotechnology Center (Madison, WI) for RNA quality and integrity evaluation by capillary electrophoresis on the Agilent 2100 Bioanalyzer platform (Agilent Technologies, Santa Clara, CA). The sequencing library from mRNA was prepared using TruSeq Stranded mRNA Library Preparation Kit (Illumina, San Diego, CA). RNAseq was carried out using Illumina NovaSeq S1 platform. Bioinformatic analysis of RNAseq reads adheres to ENCODE guidelines and best practices for RNAseq (7). Briefly, alignment of adapter-trimmed [Skewer v0.1.123 (20)] 2 × 150 (paired-end, PE) bp strand-specific Illumina reads to the Rattus norvegicus Rnor_6.0 genome (assembly accession GCA_000001895.4) was achieved with the Spliced Transcripts Alignment to a Reference software [v2.5.3a (9)], a splice-junction aware aligner, using Ensembl annotation. Expression estimation was conducted using RSEM v1.3.0 [RNAseq by expectation maximization (31)]. The raw data in the form of BAM files and normalized TPM (transcripts per million mapped reads) values have been deposited to the NCBI Gene Expression Omnibus (GEO) database and assigned accession number (GSE148453).

To test for differential expression among individual group contrasts, expected read counts were used as input into edgeR [v3.16.5 (49)]. Significance of the negative binomial test was adjusted with a Benjamini–Hochberg false discovery rate correction at the 5% level (46). Before statistical analysis with edgeR, independent filtering was performed, requiring a threshold of least two reads per million in at least three samples. The validity of the Benjamini–Hochberg false discovery rate multiple testing procedure was evaluated by inspection of the uncorrected *P* value distribution. False discovery rate at the 5% level was considered statistically significant.

Real-time RT polymerase chain reaction analysis. From the RNA isolated for RNAseq, 1 μg of RNA was reverse transcribed into cDNA using a High Capacity cDNA Reverse Transcription Kit (Applied Biosystems, Foster City, CA) as performed previously (6). Real-time PCR was performed using TaqMan Gene Expression Master Mix and TaqMan assay primers (Table 1) according to the manufacturer's instructions (Invitrogen Life Technologies, Carlsbad, CA). All PCRs were performed using the Applied Biosystems StepOne Plus Real-Time PCR System (Foster City, CA). Changes in mRNA expression were determined by the comparative threshold cycle method (34). Data were normalized to *Hprt1* and expressed as fold change compared with the female WT Sham group.

Western blot analysis. Female RV tissues were processed for Western blot analysis as previously performed (32). RV tissue was lysed in RIPA buffer (Santa Cruz Biotechnology, Santa Cruz, CA) supplemented with 1:100 HALT protease and phosphatase inhibitor cocktail (Thermo Fisher Scientific, Waltham, MA). 50 μg of each sample was separated on 4%–12% SDS-PAGE gels, transferred onto a PVDF membrane, blocked in 5% milk with 0.1% Tween-20, and immunoblotted overnight. The primary antibodies used were Mmp9 (sc-393859, Santa Cruz Biotechnology, Santa Cruz, CA), Timp1 (ab61224, Abcam, Cambridge, UK), kallikrein 10 (PA5–109887, Life Technologies, Carlsbad, CA), c-Jun (sc-74543, Santa Cruz Biotechnology), and Vinculin (sc-25336, Santa Cruz Biotechnology). Nonspecific bands for Mmp9, Timp1, and Klk10 were consistent with representative blots reported by the manufacturers. Membranes were washed and incubated in the appropriate horseradish peroxidase (HRP) secondary antibody. Immunoblots were developed with ECL Western blotting substrate (Thermo Fisher Scientific, Waltham, MA) and imaged with Bio-Rad ChemiDoc MP (Hercules, CA). Band intensity was quantitated using NIH ImageJ software.

Statistical analysis. All values are presented as means ± SE. ANOVA with Bonferroni multiple comparison correction was performed to determine differences due to genotype (ERαMut vs. WT), sex (female vs. male), and stress (PAB vs. Sham). For experiments using only female samples, two-way ANOVA was performed to determine differences due to genotype and stress. All statistical analyses were performed using IBM SPSS Statistics Version 22 (Armonk, NY). A *P* value of less than 0.05 was considered statistically significant.

RESULTS

ERα mutants demonstrate elevated serum estrogen and no sex-dependent difference in bodyweight. 17β-Estradiol levels in the serum of male and female WT (Sham and PAB) rats were physiologically consistent with those reported previously in WT (15, 27) (Fig. 1*A*). Interestingly, serum estradiol levels were increased dramatically in female sham and PAB ERαMut rats

Table 1. *Overview of primers used*

Gene	TaqMan Assay	Protein
Hprt1	Rn01527840_m1	Hypoxanthine phosphoribosyltransferase 1
Col1a1	Rn01463848_m1	Collagen type I-α1 chain
Col3a1	Rn01437681_m1	Collagen type III-α1 chain
Mmp9	Rn00579162_m1	Matrix metallopeptidase 9
Timp1	Rn01430873_g1	TIMP metallopeptidase inhibitor 1
Klk10	Rn01475770_g1	Kallikrein-related peptidase 10
Jun	Rn99999045_s1	Jun proto-oncogene

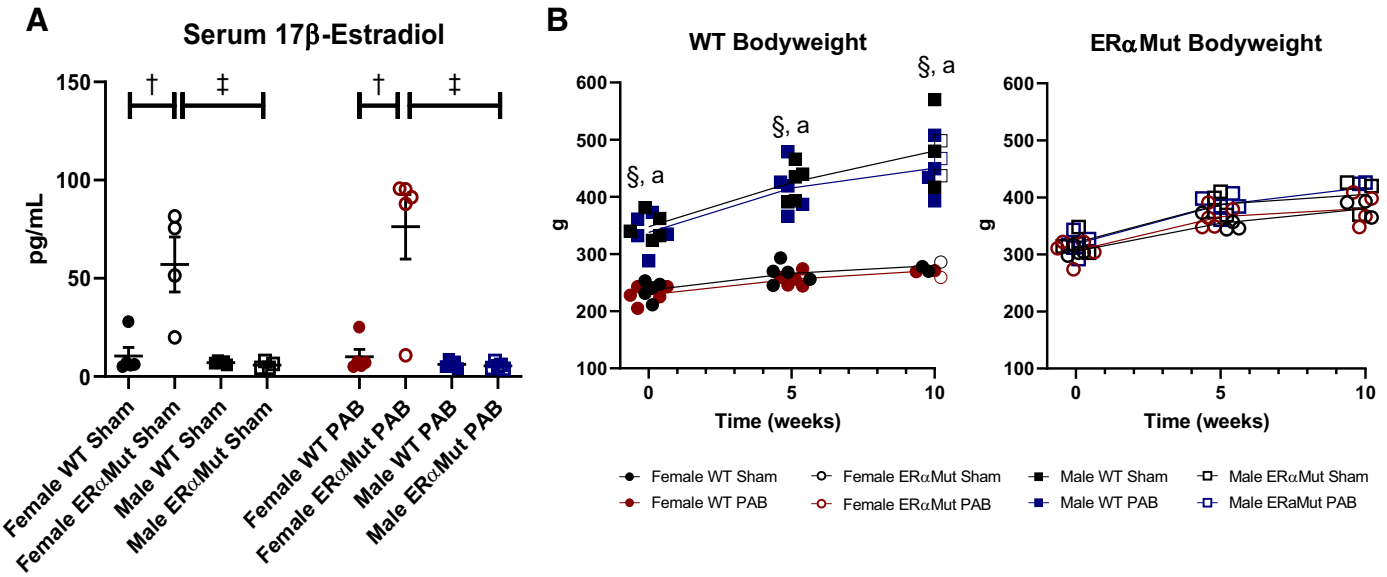

Fig. 1. Phenotypic characteristics of ERα mutant rats. Effects are shown of sex, loss of functional ERα, and PAB on serum 17β-estradiol levels (*A*) and bodyweight (*B*). Note the elevated levels of serum 17β-estradiol in female ERα mutant rats regardless of stress and the increase in bodyweight in female ERα mutant rats, with comparable bodyweight between male and female ERα mutant rats. Data are presented as means ± SE. †$P < 0.05$ ERαMut vs. WT of same sex and stress (two-way ANOVA with Bonferroni test for multiple comparison); §$P < 0.05$ Sham: female vs. male at same time point and $^{a}P < 0.05$ PAB: female vs. male at same time point (repeated-measures ANOVA with Bonferroni post hoc correction). $n = 3-5$ for each group. ERα, estrogen receptor α; ERαMut, loss-of-function mutation of ERα; PAB, pulmonary artery banding; WT, wild type.

(Fig. 1*A*). Bodyweight was greater in male WT rats than female WT rats as reported previously (15, 27) (Fig. 1*B*). However, this difference was lost in ERαMut rats, where bodyweight was similar in males and females (Fig. 1*B*). Specifically, bodyweight was greater in female ERαMut rats compared with female WT rats; bodyweight was less in male ERαMut rats compared with male WT rats (Fig. 1*B*).

PAB leads to RV-pulmonary vascular uncoupling and diastolic dysfunction in female ERα mutants. After 10 wk of PAB, RV hypertrophy measured by increased RV/TL (Fig. 2*A*), RV/BW (Fig. 2*B*), Fulton index (Fig. 2*C*), and myocyte cross-sectional area (Fig. 2*D*) was observed in all PAB groups except in the male ERαMut, where this response was less consistent. This lack of a consistent hypertrophic response in the male ERαMut rats following PAB was accompanied by a lack of increase in RV Pes (Fig. 3*A*) and a reduction in heart rate (Fig. 3*F*) despite comparable degree of constriction, suggesting inability to generate enough RV mass and to develop a sufficient contractile response. In response to PAB, the load-dependent contractility metric dP/dt_{max} was enhanced in the female ERαMut rats (Fig. 3*B*), likely contributing to their higher RV Pes compared with the female WT rats (Fig. 3*A*). Despite the increase in RV contractility, RV-pulmonary vascular coupling, as measured by E_{es}/E_a, was reduced in the female ERαMut PAB rats compared with the female WT PAB rats (Fig. 3*C*), suggesting an insufficient increase in contractility in response to the increased afterload. Uncoupling in female ERαMut rats with PAB was accompanied by impaired RV diastolic function, as evidenced by a significantly increased Tau Weiss (Fig. 3*D*). These hemodynamic changes occurred independent of systemic pressure (Fig. 3*E*) and heart rate (Fig. 3*F*), which were unchanged in female WT and ERαMut rats. Taken together, these findings suggest that female ERαMut rats are less adapted to PAB compared with female WT rats.

Female PAB ERα mutant rats exhibit smaller mitochondria in the RV, although RV mitochondrial content and respiration remain unaltered by PAB or loss of functional ERα. The significant role ERα plays in stimulating the function of skeletal muscle mitochondria (47) prompted us to investigate the possible role of ERα in RV mitochondrial adaptation to pressure overload. Mitochondrial content measured as the number of mitochondria in the RV (Fig. 4*B*) was not altered by sex, genotype, or stress. Although mitochondrial size was not affected by PAB, it was reduced in the female (but not the male) ERαMut PAB rats (Fig. 4*C*). Furthermore, despite the smaller mitochondria size in the female ERαMut PAB rats, mitochondrial respiration in RV tissue was not altered (Table 2), suggesting that the smaller sized mitochondria were well adapted to the pressure overload. Together with the hemodynamic data, these results suggest that cardiopulmonary uncoupling and diastolic dysfunction in the female ERαMut rats occurred independently of alterations in mitochondrial content and respiration.

PAB leads to greater degree of thick collagen fibers in female ERα mutant rats. Given the prominent role of fibrosis in mediating contractile performance (63) and diastolic function (44), we sought to determine the role of ERα in RV collagen content in the setting of PAB. Excessive interstitial fibrosis was observed in the female ERαMut PAB group (Fig. 5*C*). Consistent with the trends observed with Tau Weiss, none of the other groups demonstrated evidence of increased collagen deposition. Since collagen fiber size and organization into thick, tightly packed collagen and thin, loosely aligned collagen fibers contribute to material stiffness and elasticity, respectively, as well as diastolic function (19), we quantified each of these in the RV under polarized light. Compared with the female PAB WT, there were more thick collagen fibers (Fig. 5*D*) as well as thin collagen fibers (Fig. 5*E*) in female PAB ERαMut rats. On the other hand, collagen fibers in male ERαMut rats were organized

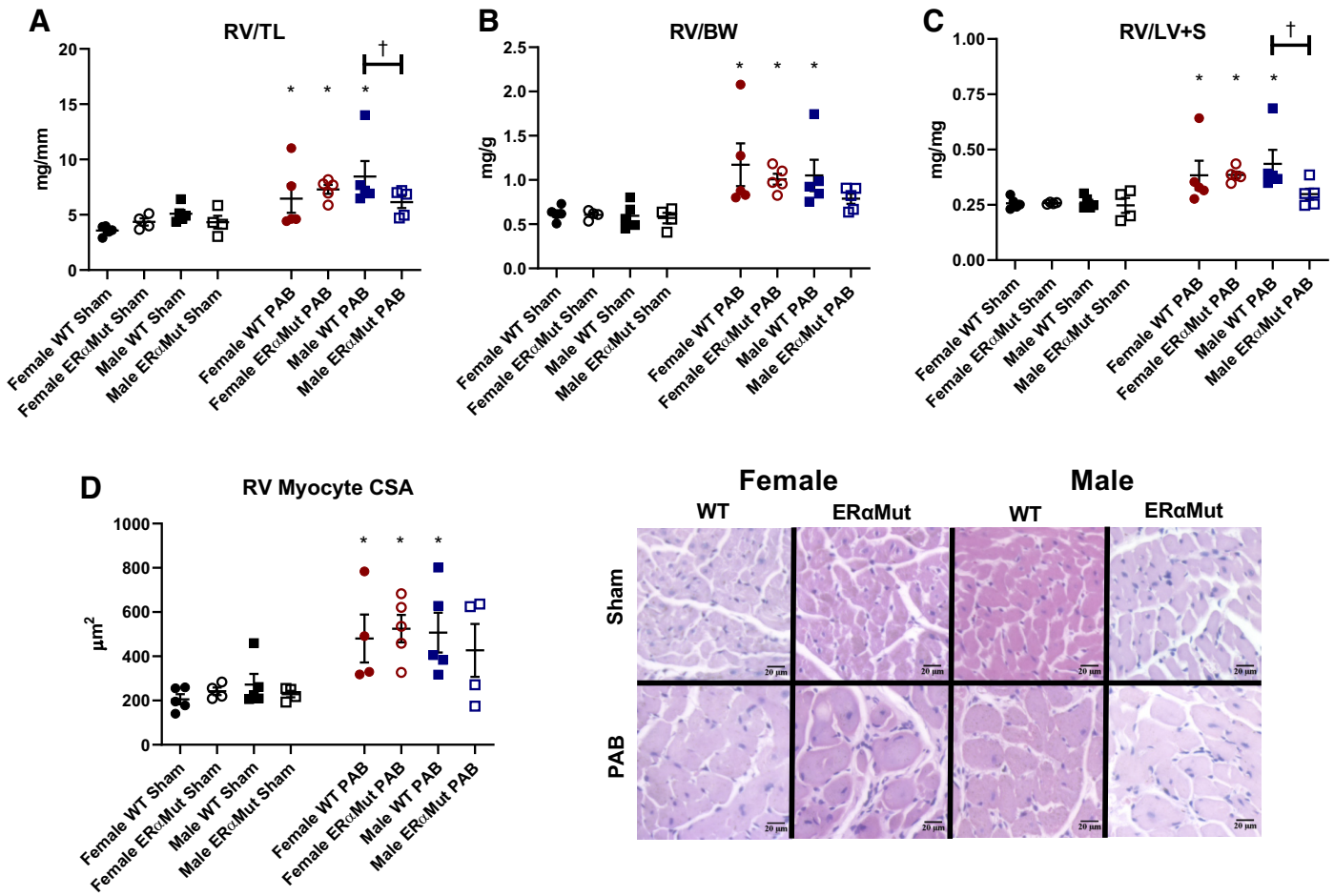

Fig. 2. PAB leads to RV hypertrophy in all PAB rats except for male ERα mutant PAB. Effects of sex, loss of functional ERα, and PAB on RV hypertrophy expressed as RV weight scaled to tibia length (TL) (*A*), RV weight scaled to bodyweight (BW) (*B*), RV weight scaled to left ventricular and septal weights (LV + S) (*C*), and RV myocyte cross-sectional area (CSA) (*D*). Note the consistent increase in the indices of RV hypertrophy observed in WT PAB and female ERα mutant PAB rats. *D* (*right*): representative images depict hematoxylin and eosin stained RV tissue in female and male WT and ERαMut rats (hematoxylin staining nuclei in blue, eosin staining cytoplasm in pink). Data are presented as means ± SE. $^*P < 0.05$ PAB vs. Sham of same sex and genotype and $\dagger P < 0.05$ ERαMut vs. WT of same sex and stress (two-way ANOVA with Bonferroni test for multiple comparison). $n = 4–5$ for each group. ERα, estrogen receptor α; ERαMut, loss-of-function mutation of ERα; PAB, pulmonary artery banding; RV, right ventricular; WT, wild type.

into more of the thin collagen fibers in response to PAB, suggesting a more compliant RV chamber. No significant difference in collagen content was observed between male PAB ERαMut and male PAB WT, which together with the organization of collagen into thin collagen fibers may explain for the preserved diastolic function in male ERαMut PAB rats. To summarize, female, but not male, ERαMut PAB rats exhibited increased collagen with increases in both thick and thin collagen fibers, suggesting collagen accumulation as a contributor to their ventricular-vascular uncoupling and diastolic dysfunction.

PAB leads to 20 downregulated and 11 upregulated genes in female ERα mutant rats compared with female WT rats. To identify genes regulated by ERα that may explain for the dysfunction and increased fibrosis in the female ERαMut RVs, we performed RNAseq in RV homogenates from female ERαMut and WT rats. In response to PAB, ERαMut displayed 20 downregulated genes (Table 3) and 11 upregulated genes (Table 4) compared with WT (Fig. 6). As expected, *Esr1*, the gene encoding for ERα, was significantly downregulated in ERαMut rats. Furthermore, we found downregulation of two genes associated with both estrogen signaling and cardiac fibrosis: kallikrein-related peptidase 10 (Klk10), a serine protease (35, 68), and Jun Proto-Oncogene (Jun), a component of the activator protein 1 transcription factor complex (58, 70). *Esr2*, the gene encoding for ERβ, and *Gper1*, the gene encoding for G protein-coupled estrogen receptor 1 (a nongenomic estrogen receptor), were unaltered by genotype or stress (data not shown). Down- and upregulation of genes involved with cardiac fibrosis were cysteine-rich angiogenic inducer 61 (Cyr61, also known as Ccn1), a secretory protein expressed at sites of wound healing (37), and suppressor of cytokine signaling 3 (Socs3), an inflammatory protein (40), respectively. The direction of their gene regulation suggests promotion of cardiac fibrosis. Interestingly, there was also down- and upregulation of genes in the tissue inhibitor of matrix metalloproteinase (TIMP) family that are involved in extracellular matrix (ECM) remodeling (13). Specifically, we observed a downregulation of *Timp4* and upregulation of *Timp1*. The direction of their opposing trends has been associated with increased collagen content in the setting of LV pressure overload (72). Moreover, we found upregulation of pentraxin-3 (Ptx3), a mediator of innate immunity that has been reported to be correlated with RV mass and end-diastolic

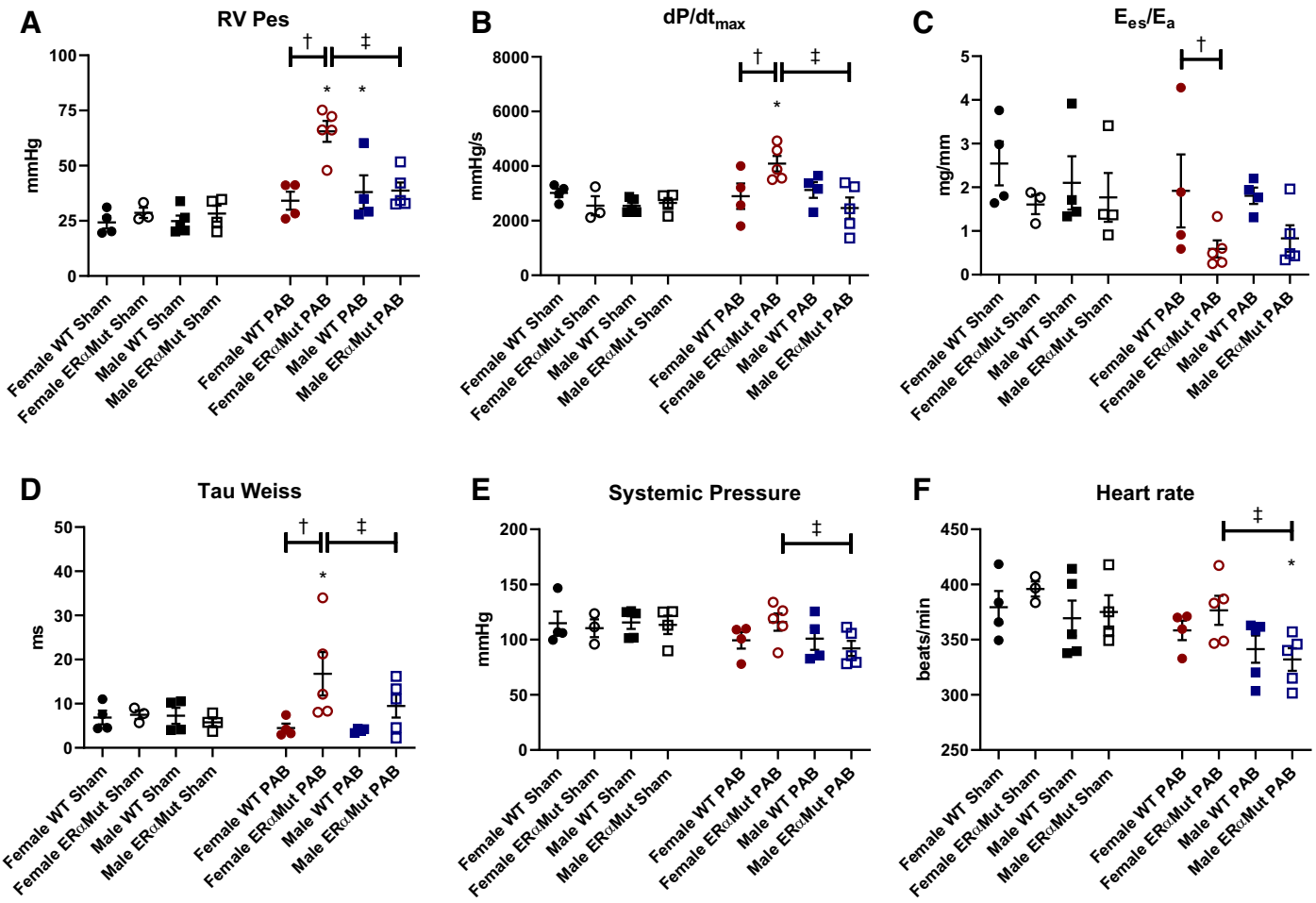

Fig. 3. Loss of functional ERα leads to adverse RV response after PAB. Effects of sex, mutation of ERα, and PAB on RV end-systolic pressure (Pes) (*A*), load-dependent RV contractility (dP/dt_{max}) (*B*), RV-pulmonary vascular coupling (E_{es}/E_a) (*C*), diastolic function (Tau Weiss) (*D*), systemic pressure (*E*), and heart rate are shown (*F*). Note the significant decrease in E_{es}/E_a and increase in Tau Weiss in the female ERαMut PAB rats. Data are presented as means ± SE. *$P < 0.05$ PAB vs. Sham of same sex and genotype, †$P < 0.05$ ERαMut vs. WT of same sex and stress, and ‡$P < 0.05$ female vs. male of same stress and genotype (two-way ANOVA with Bonferroni test for multiple comparison). $n = 3$–5 for each group. ERα, estrogen receptor α; ERαMut, loss-of-function mutation of ERα; PAB, pulmonary artery banding; RV, right ventricular; WT, wild type.

volume in patients with PAH (30). There were no differentially expressed genes involved in common pathways related to mitochondrial organization/structure or respiration (data not shown), consistent with the lack of mitochondrial content and functional changes with PAB. However, dual-specificity phosphatase 1 (Dusp1, also known as MAPK phosphatase), an enzyme with diverse functions including its novel role in regulating muscle metabolism and mitochondrial biogenesis (29), was found to be downregulated.

Interestingly, significant downregulation of genes involved in immunity was observed including *N*-deacetylase/*N*-sulfotransferase-2 (Ndst2), which encodes for an enzyme that plays a role in the biosynthesis of extracellular heparan sulfate proteoglycans (16), and a major histocompatibility complex RT1 class II, locus DMa (RT1-Dma) that is directly involved in antigen presentation for immune cells (17).

Separate comparisons for assessing effects of PAB on the transcriptome in female WT or ERαMut rats are presented in Supplemental Table S1 (see https://doi.org/10.6084/m9.figshare.12101892).

Real-time RT-PCR confirms myocardial fibrosis in female ERα mutant PAB rats is not associated with changes in Col1a1, Col3a1, or Mmp9 gene expression but is associated with decreased Klk10 and Jun gene expression. Real-time RT-PCR was performed to validate positive and negative RNAseq results. *Hprt1* was chosen as a housekeeping gene due to the comparable expected gene counts across all animals by RNAseq (data not shown). Collagen types I and III, encoded by *Col1a1* and *Col3a1*, respectively, are incorporated into thick and thin collagen fibers (8), yet were not differentially altered by RNAseq, which was confirmed by real-time RT-PCR (Fig. 7, *A* and *B*). This result suggests that collagen synthesis was comparable in all groups. The lack of change in gene expression for matrix metalloproteinase 9 (*Mmp9*), one of the gelatinases responsible for cleaving collagen, was confirmed by real-time RT-PCR (Fig. 7*C*), suggesting that *Mmp9* was not responsible for the increase in RV fibrosis. Thus, despite their known role in mediating collagen turnover, changes in *Col1a1*, *Col3*a1, and *Mmp9* gene expressions do not explain the fibrosis observed in the female ERαMut rats. On the other hand, similar to RNAseq, which demonstrated a significant

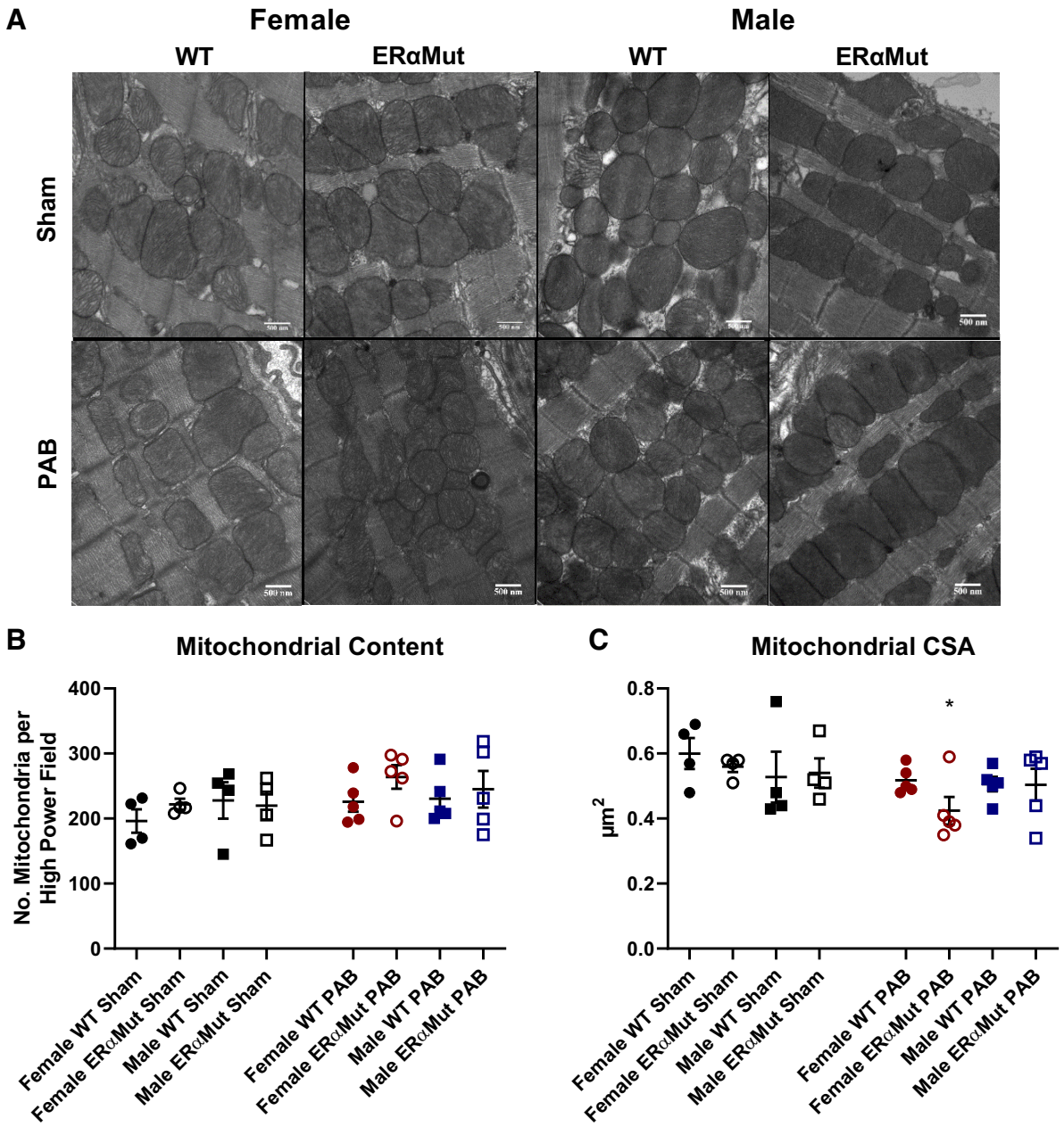

Fig. 4. Loss of functional ERα reduces RV mitochondrial size in females with PAB. Effects of sex, ERα mutation, and PAB on mitochondrial content (the number of mitochondria) (*B*) and mitochondrial cross-sectional area (CSA) (*C*) are shown. Note the lack of change in mitochondrial content across all groups in response to PAB and the reduced mitochondrial size only in the female ERαMut rats. *A*: representative electron micrographs are shown of the mitochondria in the RV tissue at ×25,000 magnification. Data are presented as means ± SE. *$P < 0.05$ PAB vs. Sham of same sex and genotype (two-way ANOVA with Bonferroni test for multiple comparison). n = 4−5 for each group. ERα, estrogen receptor α; ERαMut, loss-of-function mutation of ERα; PAB, pulmonary artery banding; RV, right ventricular.

upregulation of *Timp1*, real-time RT-PCR analysis revealed a strong trend of increase in *Timp1* in the female ERαMut PAB rats (Fig. 7*D*). However, in this limited number of animals, this did not reach statistical significance.

The lack of mRNA expression changes in the common genes involved in ECM remodeling and fibrosis formation prompted us to survey other genes associated with cardiovascular function. Real-time PCR confirmed the downregulation of *Klk10* (Fig. 8*E*) and *Jun* (Fig. 8*F*) in female ERαMut compared with female WT rats with PAB, suggesting that ERα regulates both the kallikrein-kinin pathway and Jun signaling in the RV during pressure overload.

PAB in female ERα mutant rats increases the ratio of Timp1 to Mmp9 protein expression. Western blot analysis was performed to evaluate the effects of changes in gene expression. Mmp9 protein expression was reduced with ERα mutation in sham rats and remained reduced with PAB (Fig. 8*A*). PAB did not alter Mmp9 expression in either WT or ERαMut rats. On the other hand, Timp1 protein expression was increased with ERα mutation, which was further increased with PAB (Fig. 8*B*). The increase in Timp1 expression with PAB in ERαMut rats was slightly greater than the increase in WT rats. Since increased Timp1 and decreased Mmp9 may synergistically lessen collagen degradation, we quantified the ratio of Timp1 to

Table 2. *Effects of PAB on mitochondrial oxidative phosphorylation*

Condition	Glutamate + Malate			Succinate	TMPD
	State 4, pmol/s/mg	State 3, pmol/s/mg	RCR	Complex II, pmol/s/mg	Complex IV, pmol/s/mg
WT					
Sham	20.9 ± 1.3	51.0 ± 5.7	2.4 ± 0.1	190.4 ± 26.0	436.6 ± 67.3
PAB	20.0 ± 1.4	49.6 ± 4.3	2.5 ± 0.1	204.9 ± 47.8	543.9 ± 147.9
ERαMut					
Sham	21.8 ± 1.5	54.5 ± 6.7	2.5 ± 0.1	213.9 ± 39.4	522.3 ± 87.1
PAB	18.1 ± 1.5	46.7 ± 4.1	2.6 ± 0.2	200.9 ± 29.0	504.9 ± 42.2

Values are means ± SE; $n = 5–8$ in each group with male and female rats combined within their respective genotype or stress group). RCR, respiratory control ratio; ERαMut, loss-of-function mutation of ERα; TMPD, *N,N,N′,N′*-tetramethyl-*p*-phenylenediamine; WT, wild type. Two-way ANOVA with Bonferroni test for multiple comparison was performed, but no statistical significance was found for the effect of sex, genotype, or pulmonary artery banding (PAB).

Mmp9 and found that mutation of ERα was associated with an increase in this ratio at baseline and in the setting of PAB (Fig. 8*C*). These results suggest that ERα mutation lessens collagen degradation via the combined modulation of Mmp9 and Timp1. This may explain the histological increase in collagen in the ERαMut rats with PAB.

Although we expected confirmation for RT-PCR results, we did not observe any statistical significance in Klk10 (Fig. 8*D*) or

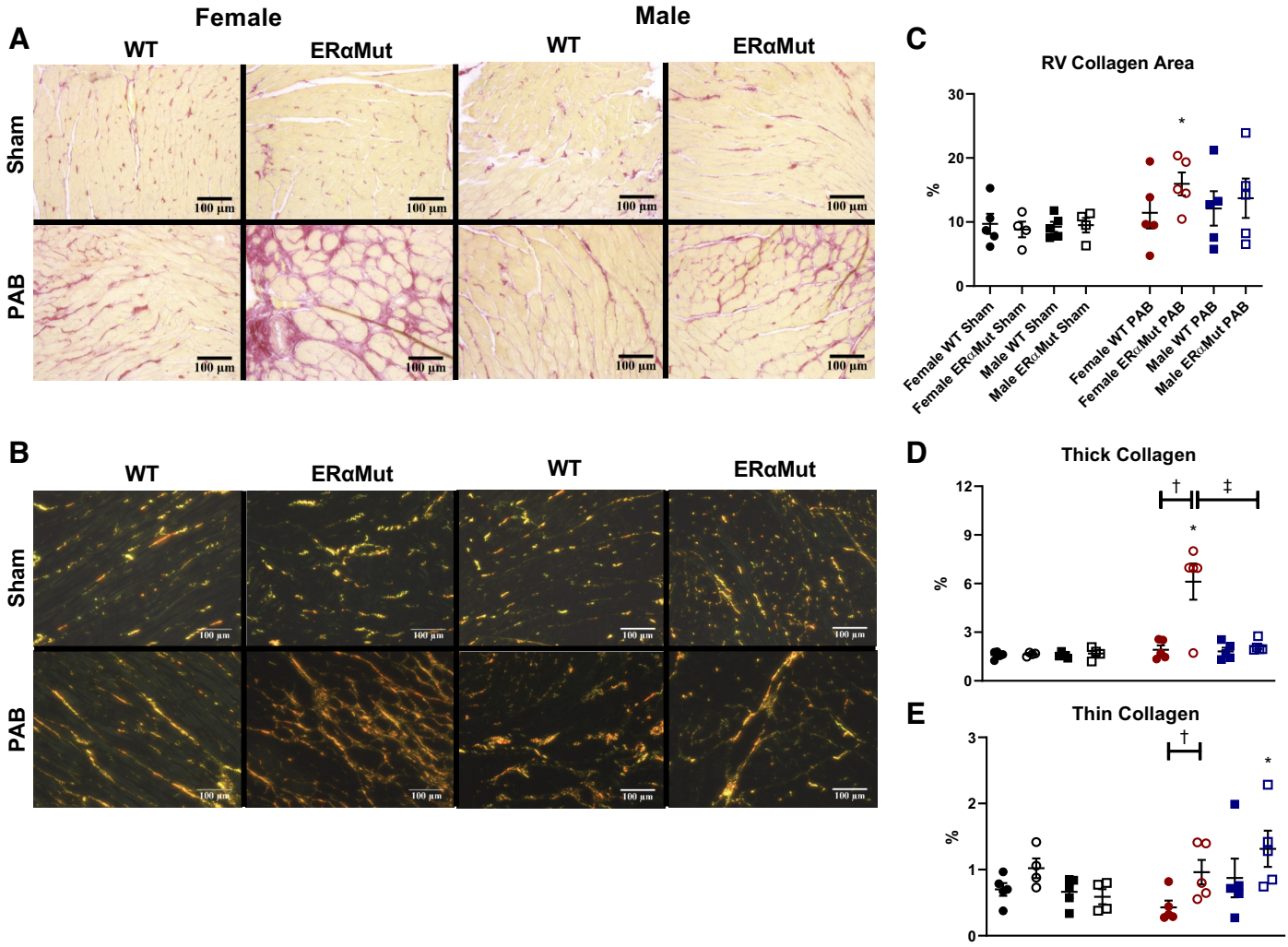

Fig. 5. Loss of functional ERα leads to excessive RV interstitial collagen content in female PAB rats. Effects of sex, mutation in ERα, and PAB on RV interstitial collagen area (*C*), RV collagen type I area (*D*), and RV collagen type III area are shown (*E*). *A* and *B*: representative bright-field (*A*) and polarized images (*B*) are shown of the interstitial collagen in the RV at ×20 magnification. Collagen was stained with picrosirius red; collagen area was calculated as ratio of the area positive for collagen (stained in pink) to the total tissue area (stained as yellow). Collagen types I and III were identified as different interference colors under polarized light, with collagen type I represented by areas of yellow, orange, or red color, and collagen type III represented by areas of green color. Note the consistent increase in collagen content for female ERαMut PAB. Data are presented as means ± SE. *$P < 0.05$ PAB vs. Sham of same sex, †$P < 0.05$ ERαMut vs. WT of same sex and stress, and ‡$P < 0.05$ female vs. male of same stress and genotype (two-way ANOVA with Bonferroni test for multiple comparison). $n = 4–5$ for each group. ERα, estrogen receptor α; ERαMut, loss-of-function mutation of ERα; PAB, pulmonary artery banding; RV, right ventricular; WT, wild type.

Table 3. *Downregulated genes compared with female WT PAB in female ERαMut PAB*

Category	Symbol	Description	LogFC	FDR
Estrogen signaling	Esr1	Estrogen receptor 1	−3.335	1.36 E-15
Estrogen signaling	Klk10	Kallikrein-related peptidase 10	−3.481	0.003
Estrogen signaling	Zfp366	Zinc finger protein 366	−1.395	0.034
Transcription factor	Fos	Fos proto-oncogene, AP-1 transcription factor subunit	−1.821	4.17 E-04
Transcription factor	Jun	Jun proto-oncogene, AP-1 transcription factor subunit	−1.052	1.38 E-09
Immunity	RT1-DMa	RT1 class II, locus DMa	−5.561	4.17 E-04
Immunity	Ndst2	*N*-deacetylase and *N*-sulfotransferase 2	−5.069	0.014
Cell cycle	Cyr61	Cysteine-rich, angiogenic inducer, 61	−1.478	1.38 E-09
Cell cycle	Btg2	BTG antiproliferation factor 2	−0.887	0.002
Transport	Calhm5	Calcium homeostasis modulator family member 5	−1.339	0.039
Transport	Arc	Activity-regulated cytoskeleton-associated protein	−1.045	0.001
ECM remodeling	Timp4	TIMP metallopeptidase inhibitor 4	−0.863	0.07
Metabolism	Cbr1	Carbonyl reductase 1	−1.132	0.0498
Metabolism	Dusp1	Dual specificity phosphatase 1	−0.766	0.003
Metabolism	Isoc2b	Isochorismatase domain containing 2b	−0.653	4.17 E-04
Cell growth	Limd1	LIM domains containing 1	−0.621	0.001
Cell growth	Spry4	Sprouty RTK signaling antagonist 4	−0.6	0.01
MISC	Otud1	OTU deubiquitinase 1	−1.194	5.37 E-05
MISC	Fam78b	Family with sequence similarity 78, member B	−1.079	0.006
MISC	Nap1l5	Nucleosome assembly protein 1-like 5	−1.024	0.019

n = 4 for each group. ERαMut, loss-of-function mutation of ERα; FC, fold change; FDR, false discovery rate; PAB, pulmonary artery banding; WT, wild type.

c-Jun (Fig. 8*E*) protein expression. However, we noted a tendency for both parameters to be decreased in ERαMut rats.

DISCUSSION

This study demonstrates that loss of functional ERα impairs the adaptive response of the female RV to pressure overload. Despite comparable constriction, female ERαMut rats exhibited significant uncoupling of the RV-pulmonary vascular circuit and diastolic dysfunction compared with female WT rats. Although mitochondrial size was decreased in female PA-banded ERαMut rats, mitochondrial respiration was preserved, suggesting that uncoupling is not due to mitochondrial dysfunction. On the other hand, female ERαMut PAB rats demonstrated excessive myocardial fibrosis (composed predominantly of thick collagen fibers), indicating adverse RV remodeling. Downregulation of *Klk10* and *Jun* alongside increased ratio of Timp1 to Mmp9 protein expression in the RVs of female ERαMut PAB rats compared with female WT PAB rats suggests that these mediators may have potential roles in the ERα-regulated pathway that prevents RV fibrosis during pressure overload. In contrast, male ERαMut rats exhibited a response to pressure overload that was almost identical to that of the male WT rats.

The ERαMut phenotype and RV hypertrophic response to afterload are consistent with prior findings in ERα KO rodents. The high level of plasma estrogen in the female ERαMut rats has been observed in a different ERα KO rat model generated by zinc finger nuclease-mediated genome editing (52). Similarly, comparable bodyweights of male and female ERαMut rats have also been reported (52). Furthermore, in response to PAB, the similar degree of RV hypertrophy seen in female ERα mutants and WT rats suggests that ERα does not attenuate hypertrophy in female animals, consistent with prior findings in female ERα KO mice with LV pressure overload (2, 55). The consistency of our findings with other reports in ERα KO rodents therefore confirms the loss of function of ERα in the rat model used for this study.

Sex differences in RV adaptation have not yet been investigated using a model of RV pressure overload that is independent of alterations in the pulmonary vasculature. However, our findings align with those reported in LV adaptation induced by LV pressure overload (53). Specifically, Ruppert et al. report that female and male rats at the stage of LV adaptative remodeling

Table 4. *Upregulated genes compared with female WT PAB in female ERαMut PAB*

Category	Symbol	Description	LogFC	FDR
Inflammation	Socs3	Suppressor of cytokine signaling 3	1.347	0.019
Immunity	Ptx3	Pentraxin 3	3.654	0.008
Immunity	Slfn4	Schlafen 4	1.626	0.012
ECM remodeling	Timp1	TIMP metallopeptidase inhibitor 1	1.192	0.006
Calcium handling	Sln	Sarcolipin	2.875	0.008
Bone formation	Tmem119	Transmembrane protein 119	2.819	0.001
Iron homeostasis	Hamp	Hepcidin antimicrobial peptide	1.918	0.001
Metabolism	Hsd11b1	Hydroxysteroid 11-beta dehydrogenase 1	0.625	0.026
Metabolism	Gfpt2	Glutamine-fructose-6-phosphate transaminase 2	0.931	0.008
MISC	Uap1	UDP-*N*-acetylglucosamine pyrophosphorylase 1	0.798	4.19 E-04
MISC	Atp8b1	ATPase phospholipid transporting 8 B1	0.551	0.032

n = 4 for each group. ERαMut, loss-of-function mutation of ERα; FC, fold change; FDR, false discovery rate; PAB, pulmonary artery banding; WT, wild type.

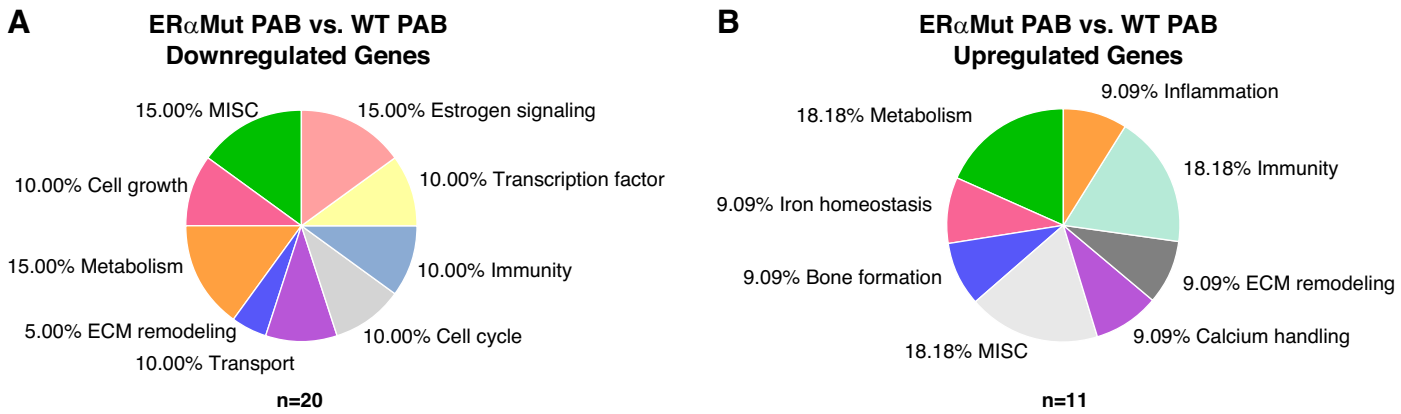

Fig. 6. Effects of loss of functional ERα on the RV transcriptome. A total of 31 differentially expressed genes between female ERαMut PAB and female WT PAB rats. Effects of ERα mutation on female PAB RVs are separated by downregulated (total genes: 20) (*A*) and upregulated (total genes: 11) genes (*B*). False discovery rate is <0.05. $n = 4$ for each of the groups. ERα, estrogen receptor α; ERαMut, loss-of-function mutation of ERα; PAB, pulmonary artery banding; RV, right ventricular; WT, wild type.

induced by LV pressure overload had comparable contractility (dP/dt_{max}), ventricular-vascular coupling (E_{es}/E_a), and ventricular relaxation (tau) (53), in which we also observed in the WT RV in response to PAB. In sum, these findings demonstrate that RV adaptive remodeling in response to pressure overload is independent of sex.

To our knowledge, this is the first study to demonstrate a protective role of ERα in the female RV in a model of pressure overload with adaptive RV hypertrophy. Whereas female ERαMut rats demonstrated inferior RV-vascular interaction as evidenced by lower E_{es}/E_a compared with female WT rats in response to PAB, male ERαMut rats did not exhibit such change despite comparable PA constriction. Preserved E_{es}/E_a and mitochondrial respiration in the WT PAB rats suggest that PAB led to adaptive hypertrophy (39, 64). Although the load-independent metric of contractility or the intrinsic RV function, E_{es}, was increased with loss of functional ERα in female rats (alongside the load-dependent metric of contractility dP/dt_{max}), the lower E_{es}/E_a in female ERαMut but not female WT PAB rats indicates that this increase was not sufficient to overcome the increase in RV afterload. This suggests that a loss-of-function mutation in ERα leads to adverse RV response to pressure overload, which aligns with the protective effects of ERα on LV and RV ejection fraction (42) as well as CO (15). Thus, in the presence of pressure overload, ERα in females protects the RV by preserving RV-pulmonary vascular coupling.

The finding that only female ERαMut rats displayed ventricular-vascular uncoupling, diastolic dysfunction, and myocardial fibrosis following PAB demonstrates a novel sex-dependent role of ERα in protecting against adverse RV remodeling. The contribution of ERα to the organization of collagen fibers into thick and thin collagen fibers with pressure overload has not yet been reported. Since thick and thin collagen fibers contribute to diastolic stiffness and compliance, respectively (19), we hypothesized that diastolic dysfunction in female ERαMut is mediated through myocardial stiffening contributed by a greater degree of collagen organized into thick, tightly packed collagen bundles and less so into thin, loosely aligned collagen bundles. Support for our hypothesis was evidenced by the significant increase in thick collagen bundles, but not thin collagen bundles, in female ERαMut in response to PAB. Extensive stiffening of the RV is not inconsistent with increased RV contractility as found here and reported previously (36, 44). In contrast, male ERαMut responded to PAB by organizing interstitial collagen into thin, loosely aligned collagen fibers, which is suggestive of a more elastic, compliance chamber and likely contributed to preserved diastolic function. Together, these results demonstrate that ERα protects females against adverse RV remodeling during RV pressure overload by preserving diastolic function and limiting excessive amount of thick collagen. ERα-mediated protective signaling in the RV may be a contributor to the female survival advantage in PAH.

To investigate contributors to fibrosis observed in the female ERαMut PA-banded RVs, we assessed regulators of collagen synthesis and degradation by real-time RT-PCR. We hypothesized that an increase in histological collagen content in the female ERαMut RV would occur alongside either (1) an increase in *Col1a1* and *Col3a1*, which would support enhanced collagen synthesis, or (2) a decrease in *Mmp9*, which would support reduced collagen degradation, or both. Neither Col1a1 nor Col3a1 gene expression was altered by PAB in either the WT or ERαMut group. In the WT group, this finding aligns with the histological findings and agrees with prior work in rats (44). In the ERαMut group, collagen accumulation appears mediated by changes in degradation activity rather than synthetic activity (Fig. 8*C*). The ratio of Timp1 to Mmp9 is a more reliable determinant of collagen degradation than increases in Mmp9 or decreases in Timp1 alone (71), since they can act synergistically. The increased ratio of Timp1 to Mmp9 in female ERαMut PAB rats compared with female WT PAB rats suggests that the ERα mutation inhibits collagen degradation, which contributes to myocardial fibrosis. At the same time, due to the limitation of a single time point at which we observed fibrosis and investigated gene expression changes, it is possible that collagen synthesis contributed to fibrosis development in our model but was not captured at the terminal time point. A prior study on the progressive accumulation of collagen in LV pressure overloaded rats demonstrated a significant increase in collagen content and gene expression of *Col3a1* as early as 1 wk following pressure overload (11). However, the fibrosis and significant increase in *Col1a1* gene expression were not observed until 16 wk postsurgery, which suggest a gradual

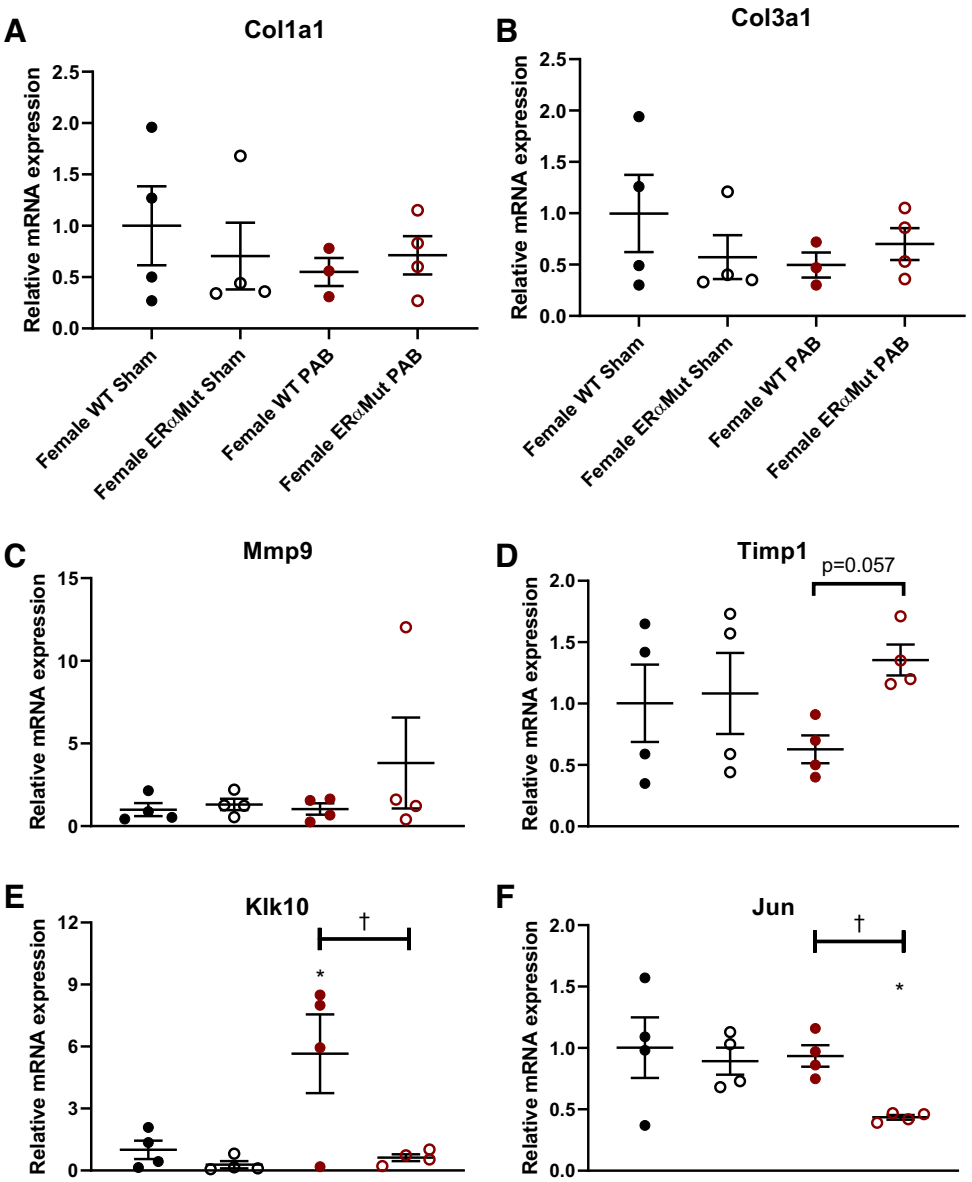

Fig. 7. Mutation in ERα tended to increase Timp1 and significantly reduced Klk10 and Jun mRNA expression in the RV in response to PAB in females. Effects of ERα mutation and PAB on female RV gene expression of Col1a1 (*A*), Col3a1 (*B*), Mmp9 (*C*), Timp1 (*D*), kallikrein-related peptidase 10 (Klk10) (*E*), and Jun (*F*) are shown. Data are presented as means ± SE. *$P < 0.05$, PAB vs. Sham of same sex, and †$P < 0.05$, ERαMut vs. WT of same sex and stress (2-way ANOVA with Bonferroni test for multiple comparison). n = 3–4 for each group. ERα, estrogen receptor α; Klk10, kallikrein-related peptidase 10; PAB, pulmonary artery banding; RV, right ventricular; WT, wild type.

accumulation of collagen (11). We speculate that in the first few weeks following PAB, there was a gradual increase in collagen synthesis and/or decrease in collagen degradation in female ERαMut rats that ceased upon sufficient structural adaptation to the afterload. However, further investigation will be required to test this hypothesis. Furthermore, conclusions about the impact of increased Timp1 to Mmp9 protein level observed in the female ERαMut PAB rats are limited by the lack of zymogenic activity measurements for Mmp9 and Timp1, which should be taken into consideration.

RNAseq was performed to globally assess additional genes involved in estrogen signaling that may explain the myocardial fibrosis in female ERαMut PAB rats. *Klk10* and *Jun* stood out because estrogen has stimulatory effect on *Klk10* gene expression (35, 41) and *Jun* has a direct interaction with ERα (58). *Klk10* codes for a serine protease that has vasodilatory action in coronary arteries (23) and aorta (12). A member of the Klk family has previously been shown to reduce cardiac fibrosis in a myocardial infarction model (1). Currently, only one study has reported increased expression of *Klk10* with decreased collagen content in a model of volume overload (68). It is important to note that a decrease in collagen content is a common response to volume overload, whereas an increase in collagen is a common response to pressure overload (73). The impact of *Klk10* downregulation in the RV during pressure overload remains unknown. Further investigation is needed to confirm whether ERα directly or indirectly increases *Klk10* and whether this modulation limits RV fibrosis during pressure overload. Furthermore, although gene expression of *Klk10* is reduced in female ERαMut PAB rats compared with female WT PAB rats, protein expression of Klk10 was comparable between the two groups, suggesting a possible role of altered zymogenic activity and post-translational modifications.

Along with *Klk10* downregulation, reduced *Jun* expression in female ERαMut PAB rats suggests alterations in various upstream targets, including MAPK and ERK1/2 signaling,

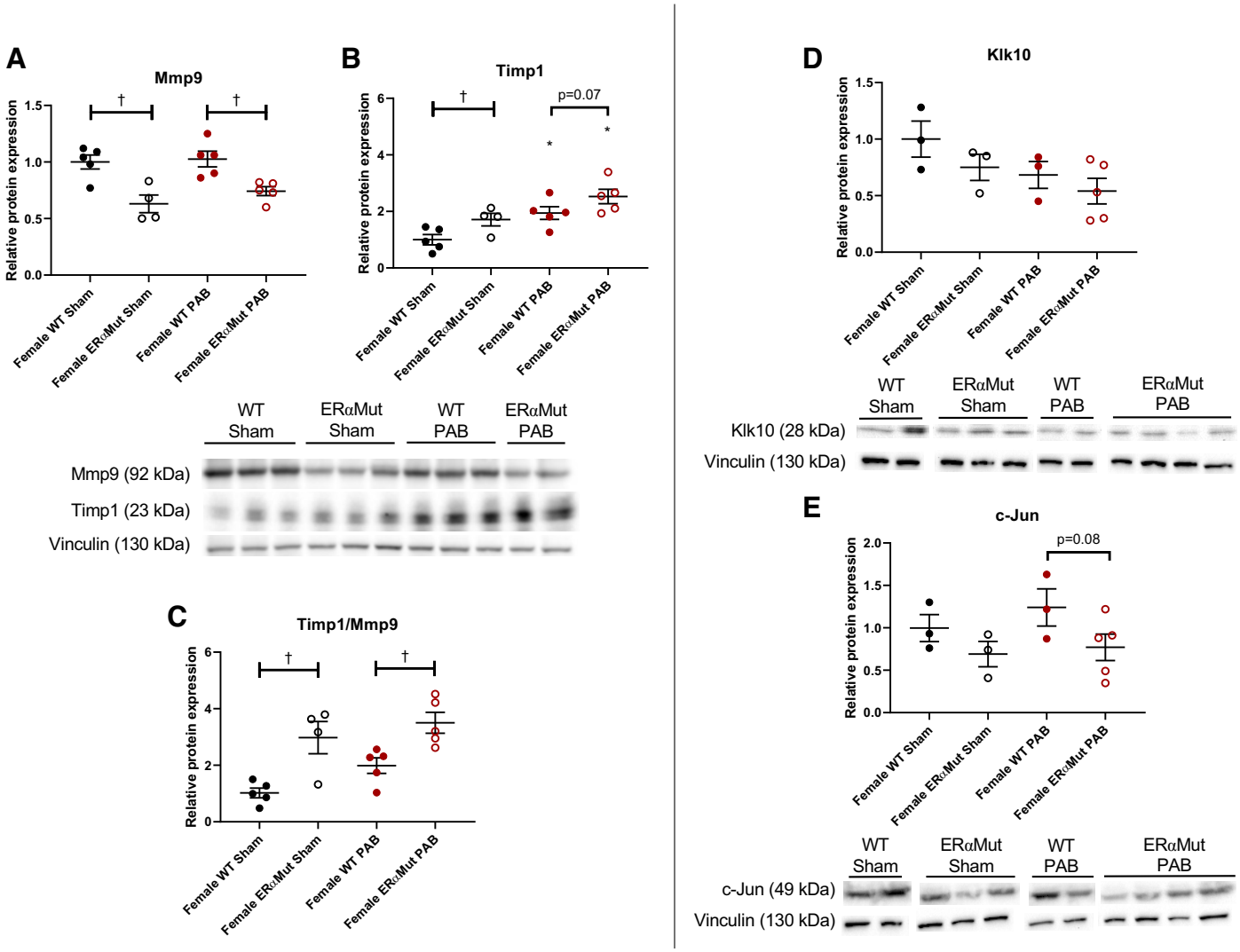

Fig. 8. ERα mutation increased the ratio of Timp1 to Mmp9 protein expression level in the female RV in response to PAB. Effects of ERα mutation and PAB on female RV protein expression of Mmp9 (*A*), Timp1 (*B*), ratio of Timp1 to Mmp9 (*C*), Klk10 (*D*), and c-Jun (*E*) are shown. Representative immunoblots are shown below the graphs and densitometry results (normalized for vinculin control and expressed as fold change vs. female WT Sham) are depicted in the graphs. Data are presented as means ± SE. **P* < 0.05, PAB vs. Sham of same sex, and †*P* < 0.05, ERαMut vs. WT of same sex and stress (2-way ANOVA with Bonferroni test for multiple comparison). *n* = 4 for each group. ERα, estrogen receptor α; Klk10, kallikrein-related peptidase 10; Mmp9, matrix metalloproteinase 9; PAB, pulmonary artery banding; RV, right ventricular; Timp1, TIMP metallopeptidase inhibitor 1; WT, wild type.

which are involved in regulating processes, such as cardiac hypertrophy, cell proliferation, and apoptosis (51). In a striated muscle-specific knockout of *Jun* in mice, *Jun* was implicated in limiting myocardial fibrosis in LV pressure overload (70), suggesting that *Jun* may also be involved in limiting RV fibrosis among other processes during pressure overload. Protein expression levels of Jun in female ERαMut PAB rats tended to agree with gene expression levels, but did not reach statistical significance likely due to the small sample size. Together with *Klk10*, increased *Jun* signaling may also be involved in mediating ERα's role in limiting excessive fibrosis during pressure overload.

Because of the significant difference in bodyweight between the female ERαMut and WT rats, we also considered the contribution bodyweight changes can have on the development of fibrosis. We investigated correlations between bodyweight gain and measures of fibrosis, such as histological percentages of collagen area, thick collagen, and thin collagen as well as gene expression levels of *Col1a1* and *Col3a1*, but did not find any statistically significant correlation between these metrics in the female ERαMut PAB rats. Whether phenotypic differences in bodyweight due to ERα mutation have a correlative relationship with the development of cardiac fibrosis in response to PAB warrants further investigation.

CONCLUSIONS

In summary, our results demonstrate that ERα protects the female RV from RV-pulmonary vascular uncoupling, diastolic dysfunction, and fibrosis due to pressure overload. Loss of functional ERα resulted in an adverse response to PAB, characterized by uncoupling of the RV-pulmonary vascular circuit. Downregulation of *Klk10* and *Jun* as well as increased ratio of Timp1 to Mmp9 protein expression in the female ERαMut PAB

rats compared with female WT PAB rats implicate *Klk10*, *Jun*, and altered balance of Timp1 to Mmp9 as potential mediators in ERα-regulated pathways in RV pressure overload. Diastolic dysfunction alongside excessive fibrosis in the female ERαMut rats suggests an important role for ERα in protecting female RV diastolic function by limiting fibrosis during pressure overload.

ACKNOWLEDGMENTS

We thank Gaoussou Diara, Allison Rodgers, Randy Massey, and C. Dustin Rubinstein for technical expertise with the surgery, echocardiography, electron microscopy, and characterization of ERα mutant rats, respectively; Dr. David Schreier, Jakob Sedlak, Tony So, Abigail Drake, and Dr. Jens Eickhoff for help with data collection and/or analysis; and UW Madison Biotechnology Center Gene Expression Center and DNA Sequencing Facility for providing library preparation and next-generation sequencing services.

GRANTS

This work was supported by National Heart, Lung, and Blood Institute Grants 1R56HL134736 and 1R01HL144727 and Veterans Affairs Merit Review Award Grant 2 I01 BX002042-05.

DISCLOSURES

No conflicts of interest, financial or otherwise, are declared by the authors.

AUTHOR CONTRIBUTIONS

T-C.C., X.S., T.L., N.C.C., J.L.P., D.T., A.L.F., and R.L. conceived and designed research; T-C.C., J.L.P., D.T., B.Y., and T.A.H. performed experiments; T-C.C., K.N.G., B.Y., and A.B. analyzed data; T-C.C., K.N.G., T.L., N. C.C., J.L.P., D.T., S.K., A.L.F., T.A.H., and A.B. interpreted results of experiments; T-C.C. prepared figures; T-C.C. drafted manuscript; T-C.C., K.N.G., T. L., N.C.C., J.L.P., D.T., and T.A.H. edited and revised manuscript; T-C.C., K.N. G., T.L., N.C.C., J.L.P., D.T., S.K., B.Y., A.L.F., T.A.H., A.B., and R.L. approved final version of manuscript.

REFERENCES

1. **Agata J**, **Chao L**, **Chao J.** Kallikrein gene delivery improves cardiac reserve and attenuates remodeling after myocardial infarction. *Hypertension* 40: 653–659, 2002. doi:10.1161/01.HYP.0000036035.41122.99.
2. **Babiker FA**, **Lips D**, **Meyer R**, **Delvaux E**, **Zandberg P**, **Janssen B**, **van Eys G**, **Grohé C**, **Doevendans PA.** Estrogen receptor beta protects the murine heart against left ventricular hypertrophy. *Arterioscler Thromb Vasc Biol* 26: 1524–1530, 2006. doi:10.1161/01.ATV.0000223344.11128.23.
3. **Bellofiore A**, **Vanderpool R**, **Brewis MJ**, **Peacock AJ**, **Chesler NC.** A novel single-beat approach to assess right ventricular systolic function. *J Appl Physiol (1985)* 124: 283–290, 2018. doi:10.1152/japplphysiol.00258.2017.
4. **Benjamin EJ**, **Muntner P**, **Alonso A**, **Bittencourt MS**, **Callaway CW**, **Carson AP**, et al**.** Heart disease and stroke statistics-2019 update: a report from the American Heart Association. *Circulation* 139: e56–e528, 2019. doi:10.1161/CIR.0000000000000659.
5. **Betz P**, **Nerlich A**, **Wilske J**, **Wiest I**, **Penning R**, **Eiseumenger W.** Comparison of the solophenyl-red polarization method and the immunohistochemical analysis for collagen type III. *Int J Legal Med* 105: 27–29, 1992. doi:10.1007/BF01371233.
6. **Cheng TC**, **Philip JL**, **Tabima DM**, **Hacker TA**, **Chesler NC.** Multiscale structure-function relationships in right ventricular failure due to pressure overload. *Am J Physiol Heart Circ Physiol* 315: H699–H708, 2018. doi:10.1152/ajpheart.00047.2018.
7. **ENCODE Project.** *ENCODE Guidelines and Best Practices for RNA-Seq: Revised December,* 2016. https://www.encodeproject.org/documents/cede0cbe-d324-4ce7-ace4-f0c3eddf5972/@@download/attachment/ENCODE%20Best%20Practices%20for%20RNA_v2.pdf
8. **Dayan D**, **Hiss Y**, **Hirshberg A**, **Bubis JJ**, **Wolman M.** Are the polarization colors of picrosirius red-stained collagen determined only by the diameter of the fibers? *Histochemistry* 93: 27–29, 1989. doi:10.1007/BF00266843.
9. **Dobin A**, **Davis CA**, **Schlesinger F**, **Drenkow J**, **Zaleski C**, **Jha S**, **Batut P**, **Chaisson M**, **Gingeras TR.** STAR: ultrafast universal RNA-seq aligner. *Bioinformatics* 29: 15–21, 2013. doi:10.1093/bioinformatics/bts635.
10. **Dworatzek E**, **Mahmoodzadeh S**, **Schriever C**, **Kusumoto K**, **Kramer L**, **Santos G**, **Fliegner D**, **Leung YK**, **Ho SM**, **Zimmermann WH**, **Lutz S**, **Regitz-Zagrosek V.** Sex-specific regulation of collagen I and III expression by 17β-Estradiol in cardiac fibroblasts: role of estrogen receptors. *Cardiovasc Res* 115: 315–327, 2018. doi:10.1093/cvr/cvy185.
11. **Eleftheriades EG**, **Durand JB**, **Ferguson AG**, **Engelmann GL**, **Jones SB**, **Samarel AM.** Regulation of procollagen metabolism in the pressure-overloaded rat heart. *J Clin Invest* 91: 1113–1122, 1993. doi:10.1172/JCI116270.
12. **Erol K**, **Sirmagul B**, **Kilic FS**, **Yigitaslan S**, **Dogan AE.** The role of inflammation and COX-derived prostanoids in the effects of bradykinin on isolated rat aorta and urinary bladder. *Inflammation* 35: 420–428, 2012. doi:10.1007/s10753-011-9331-7.
13. **Fan D**, **Takawale A**, **Lee J**, **Kassiri Z.** Cardiac fibroblasts, fibrosis and extracellular matrix remodeling in heart disease. *Fibrogenesis Tissue Repair* 5: 15, 2012. doi:10.1186/1755-1536-5-15.
14. **Frump A**, **Yakubov B**, **Hester J**, **Fisher A**, **Cook T**, **Cheng T**, **Tabima M**, **Sun X**, **Chesler N**, **Lahm T.** Loss of estrogen receptor alpha (ERα) worsens hemodynamic alterations and right ventricular (RV) adaptation in female rats with pulmonary hypertension (PH) (Abstract). Mini Symposium D96: What's New in PAH And RV Signaling: Lessons from the Best Abstracts. American Thoracic Society 2020 International Conference, 2020, A7673.
15. **Frump AL**, **Goss KN**, **Vayl A**, **Albrecht M**, **Fisher A**, **Tursunova R**, **Fierst J**, **Whitson J**, **Cucci AR**, **Brown MB**, **Lahm T.** Estradiol improves right ventricular function in rats with severe angioproliferative pulmonary hypertension: effects of endogenous and exogenous sex hormones. *Am J Physiol Lung Cell Mol Physiol* 308: L873–L890, 2015. doi:10.1152/ajplung.00006.2015.
16. **Humphries DE**, **Wong GW**, **Friend DS**, **Gurish MF**, **Qiu WT**, **Huang C**, **Sharpe AH**, **Stevens RL.** Heparin is essential for the storage of specific granule proteases in mast cells. *Nature* 400: 769–772, 1999. doi:10.1038/23481.
17. **Hurt P**, **Walter L**, **Sudbrak R**, **Klages S**, **Müller I**, **Shiina T**, **Inoko H**, **Lehrach H**, **Günther E**, **Reinhardt R**, **Himmelbauer H.** The genomic sequence and comparative analysis of the rat major histocompatibility complex. *Genome Res* 14: 631–639, 2004. doi:10.1101/gr.1987704.
18. **Jacobs W**, **van de Veerdonk MC**, **Trip P**, **de Man F**, **Heymans MW**, **Marcus JT**, **Kawut SM**, **Bogaard HJ**, **Boonstra A**, **Vonk Noordegraaf A.** The right ventricle explains sex differences in survival in idiopathic pulmonary arterial hypertension. *Chest* 145: 1230–1236, 2014. doi:10.1378/chest.13-1291.
19. **Jalil JE**, **Doering CW**, **Janicki JS**, **Pick R**, **Shroff SG**, **Weber KT.** Fibrillar collagen and myocardial stiffness in the intact hypertrophied rat left ventricle. *Circ Res* 64: 1041–1050, 1989. doi:10.1161/01.RES.64.6.1041.
20. **Jiang H**, **Lei R**, **Ding S-W**, **Zhu S.** Skewer: a fast and accurate adapter trimmer for next-generation sequencing paired-end reads. *BMC Bioinformatics* 15: 182, 2014. doi:10.1186/1471-2105-15-182.
22. **Junqueira LCU**, **Montes GS**, **Sanchez EM.** The influence of tissue section thickness on the study of collagen by the Picrosirius-polarization method. *Histochemistry* 74: 153–156, 1982. doi:10.1007/BF00495061.
23. **Kuga T**, **Mohri M**, **Egashira K**, **Hirakawa Y**, **Tagawa T**, **Shimokawa H**, **Takeshita A.** Bradykinin-induced vasodilation of human coronary arteries in vivo: role of nitric oxide and angiotensin-converting enzyme. *J Am Coll Cardiol* 30: 108–112, 1997. doi:10.1016/S0735-1097(97)00112-5.
24. **Kuznetsov AV**, **Schneeberger S**, **Seiler R**, **Brandacher G**, **Mark W**, **Steurer W**, **Saks V**, **Usson Y**, **Margreiter R**, **Gnaiger E.** Mitochondrial defects and heterogeneous cytochrome c release after cardiac cold ischemia and reperfusion. *Am J Physiol Heart Circ Physiol* 286: H1633–H1641, 2004. doi:10.1152/ajpheart.00701.2003.
25. **Kuznetsov AV**, **Veksler V**, **Gellerich FN**, **Saks V**, **Margreiter R**, **Kunz WS.** Analysis of mitochondrial function in situ in permeabilized muscle fibers, tissues and cells. *Nat Protoc* 3: 965–976, 2008. doi:10.1038/nprot.2008.61.
26. **Lahm T**, **Albrecht M**, **Fisher AJ**, **Selej M**, **Patel NG**, **Brown JA**, **Justice MJ**, **Brown MB**, **Van Demark M**, **Trulock KM**, **Dieudonne D**, **Reddy JG**, **Presson RG**, **Petrache I.** 17β-Estradiol attenuates hypoxic pulmonary hypertension via estrogen receptor-mediated effects. *Am J Respir Crit Care Med* 185: 965–980, 2012. doi:10.1164/rccm.201107-1293OC.
27. **Lahm T**, **Frump AL**, **Albrecht ME**, **Fisher AJ**, **Cook TG**, **Jones TJ**, **Yakubov B**, **Whitson J**, **Fuchs RK**, **Liu A**, **Chesler NC**, **Brown MB.** 17β-Estradiol mediates superior adaptation of right ventricular function to acute strenuous exercise in female rats with severe pulmonary hypertension. *Am J*

Physiol Lung Cell Mol Physiol 311: L375–L388, 2016. doi:10.1152/ajplung.00132.2016.

28. **Langer SF**, **Habazettl H**, **Kuebler WM**, **Pries AR.** Estimation of the left ventricular relaxation time constant tau requires consideration of the pressure asymptote. *Physiol Res* 54: 601–610, 2005.
29. **Lawan A**, **Min K**, **Zhang L**, **Canfran-Duque A**, **Jurczak MJ**, **Camporez JPG**, **Nie Y**, **Gavin TP**, **Shulman GI**, **Fernandez-Hernando C**, **Bennett AM.** Skeletal muscle-specific deletion of MKP-1 reveals a p38 MAPK/JNK/Akt signaling node that regulates obesity-induced insulin resistance. *Diabetes* 67: 624–635, 2018. doi:10.2337/db17-0826.
30. **Leary PJ**, **Jenny NS**, **Barr RG**, **Bluemke DA**, **Harhay MO**, **Heckbert SR**, **Kronmal RA**, **Lima JA**, **Mikacenic C**, **Tracy RP**, **Kawut SM.** Pentraxin-3 and the right ventricle: the Multi-Ethnic Study of Atherosclerosis-Right Ventricle Study. *Pulm Circ* 4: 250–259, 2014. doi:10.1086/675988.
31. **Li B**, **Dewey CN.** RSEM: accurate transcript quantification from RNA-Seq data with or without a reference genome. *BMC Bioinformatics* 12: 323, 2011. doi:10.1186/1471-2105-12-323.
32. **Liu A**, **Philip J**, **Vinnakota KC**, **Van den Bergh F**, **Tabima DM**, **Hacker T**, **Beard DA**, **Chesler NC.** Estrogen maintains mitochondrial content and function in the right ventricle of rats with pulmonary hypertension. *Physiol Rep* 5: e13157, 2017. doi:10.14814/phy2.13157.
34. **Livak KJ**, **Schmittgen TD.** Analysis of relative gene expression data using real-time quantitative PCR and the 2(-Delta Delta C(T)) Method. *Methods* 25: 402–408, 2001. doi:10.1006/meth.2001.1262.
35. **Luo LY**, **Grass L**, **Diamandis EP.** Steroid hormone regulation of the human kallikrein 10 (KLK10) gene in cancer cell lines and functional characterization of the KLK10 gene promoter. *Clin Chim Acta* 337: 115–126, 2003. doi:10.1016/j.cccn.2003.07.008.
36. **Mendes-Ferreira P**, **Santos-Ribeiro D**, **Adão R**, **Maia-Rocha C**, **Mendes-Ferreira M**, **Sousa-Mendes C**, **Leite-Moreira AF**, **Brás-Silva C.** Distinct right ventricle remodeling in response to pressure overload in the rat. *Am J Physiol Heart Circ Physiol* 311: H85–H95, 2016. doi:10.1152/ajpheart.00089.2016.
37. **Meyer K**, **Hodwin B**, **Ramanujam D**, **Engelhardt S**, **Sarikas A.** Essential role for premature senescence of myofibroblasts in myocardial fibrosis. *J Am Coll Cardiol* 67: 2018–2028, 2016. doi:10.1016/j.jacc.2016.02.047.
38. **Montes GS**, **Junqueira LC.** The use of the Picrosirius-polarization method for the study of the biopathology of collagen. *Mem Inst Oswaldo Cruz* 86, *Suppl* 3: 1–11, 1991. doi:10.1590/S0074-02761991000700002.
39. **Nouette-Gaulain K**, **Malgat M**, **Rocher C**, **Savineau JP**, **Marthan R**, **Mazat JP**, **Sztark F.** Time course of differential mitochondrial energy metabolism adaptation to chronic hypoxia in right and left ventricles. *Cardiovasc Res* 66: 132–140, 2005. doi:10.1016/j.cardiores.2004.12.023.
40. **Oba T**, **Yasukawa H**, **Hoshijima M**, **Sasaki K**, **Futamata N**, **Fukui D**, **Mawatari K**, **Nagata T**, **Kyogoku S**, **Ohshima H**, **Minami T**, **Nakamura K**, **Kang D**, **Yajima T**, **Knowlton KU**, **Imaizumi T.** Cardiac-specific deletion of SOCS-3 prevents development of left ventricular remodeling after acute myocardial infarction. *J Am Coll Cardiol* 59: 838–852, 2012. doi:10.1016/j.jacc.2011.10.887.
41. **Paliouras M**, **Diamandis EP.** Androgens act synergistically to enhance estrogen-induced upregulation of human tissue kallikreins 10, 11, and 14 in breast cancer cells via a membrane bound androgen receptor. *Mol Oncol* 1: 413–424, 2008. doi:10.1016/j.molonc.2008.01.001.
42. **Pelzer T**, **Jazbutyte V**, **Hu K**, **Segerer S**, **Nahrendorf M**, **Nordbeck P**, **Bonz AW**, **Muck J**, **Fritzemeier KH**, **Hegele-Hartung C**, **Ertl G**, **Neyses L.** The estrogen receptor-alpha agonist 16alpha-LE2 inhibits cardiac hypertrophy and improves hemodynamic function in estrogen-deficient spontaneously hypertensive rats. *Cardiovasc Res* 67: 604–612, 2005. doi:10.1016/j.cardiores.2005.04.035.
43. **Pesta D**, **Gnaiger E.** High-resolution respirometry: OXPHOS protocols for human cells and permeabilized fibers from small biopsies of human muscle. *Methods Mol Biol* 810: 25–58, 2012. doi:10.1007/978-1-61779-382-0_3.
44. **Rain S**, **Andersen S**, **Najafi A**, **Gammelgaard Schultz J**, **da Silva Gonçalves Bós D**, **Handoko ML**, **Bogaard HJ**, **Vonk-Noordegraaf A**, **Andersen A**, **van der Velden J**, **Ottenheijm CA**, **de Man FS.** Right ventricular myocardial stiffness in experimental pulmonary arterial hypertension: relative contribution of fibrosis and myofibril stiffness. *Circ Heart Fail* 9: e002636, 2016. doi:10.1161/CIRCHEARTFAILURE.115.002636.
45. **Rain S**, **Handoko ML**, **Trip P**, **Gan CT**, **Westerhof N**, **Stienen GJ**, **Paulus WJ**, **Ottenheijm CA**, **Marcus JT**, **Dorfmüller P**, **Guignabert C**, **Humbert M**, **Macdonald P**, **Dos Remedios C**, **Postmus PE**, **Saripalli C**, **Hidalgo CG**, **Granzier HL**, **Vonk-Noordegraaf A**, **van der Velden J**, **de Man FS.** Right ventricular diastolic impairment in patients with pulmonary arterial hypertension. *Circulation* 128: 2016–2025, 2013. doi:10.1161/CIRCULATIONAHA.113.001873.
46. **Reiner A**, **Yekutieli D**, **Benjamini Y.** Identifying differentially expressed genes using false discovery rate controlling procedures. *Bioinformatics* 19: 368–375, 2003. doi:10.1093/bioinformatics/btf877.
47. **Ribas V**, **Drew BG**, **Zhou Z**, **Phun J**, **Kalajian NY**, **Soleymani T**, **Daraei P**, **Widjaja K**, **Wanagat J**, **de Aguiar Vallim TQ**, **Fluitt AH**, **Bensinger S**, **Le T**, **Radu C**, **Whitelegge JP**, **Beaven SW**, **Tontonoz P**, **Lusis AJ**, **Parks BW**, **Vergnes L**, **Reue K**, **Singh H**, **Bopassa JC**, **Toro L**, **Stefani E**, **Watt MJ**, **Schenk S**, **Akerstrom T**, **Kelly M**, **Pedersen BK**, **Hewitt SC**, **Korach KS**, **Hevener AL.** Skeletal muscle action of estrogen receptor α is critical for the maintenance of mitochondrial function and metabolic homeostasis in females. *Sci Transl Med* 8: 334ra54, 2016. doi:10.1126/scitranslmed.aad3815.
48. **Ribas V**, **Nguyen MT**, **Henstridge DC**, **Nguyen AK**, **Beaven SW**, **Watt MJ**, **Hevener AL.** Impaired oxidative metabolism and inflammation are associated with insulin resistance in ERalpha-deficient mice. *Am J Physiol Endocrinol Metab* 298: E304–E319, 2010. doi:10.1152/ajpendo.00504.2009.
49. **Robinson MD**, **McCarthy DJ**, **Smyth GK.** edgeR: a Bioconductor package for differential expression analysis of digital gene expression data. *Bioinformatics* 26: 139–140, 2010. doi:10.1093/bioinformatics/btp616.
51. **Rose BA**, **Force T**, **Wang Y.** Mitogen-activated protein kinase signaling in the heart: angels versus demons in a heart-breaking tale. *Physiol Rev* 90: 1507–1546, 2010. doi:10.1152/physrev.00054.2009.
52. **Rumi MA**, **Dhakal P**, **Kubota K**, **Chakraborty D**, **Lei T**, **Larson MA**, **Wolfe MW**, **Roby KF**, **Vivian JL**, **Soares MJ.** Generation of Esr1-knockout rats using zinc finger nuclease-mediated genome editing. *Endocrinology* 155: 1991–1999, 2014. doi:10.1210/en.2013-2150.
53. **Ruppert M**, **Korkmaz-Icöz S**, **Loganathan S**, **Jiang W**, **Lehmann L**, **Oláh A**, **Sayour AA**, **Barta BA**, **Merkely B**, **Karck M**, **Radovits T**, **Szabó G.** Pressure-volume analysis reveals characteristic sex-related differences in cardiac function in a rat model of aortic banding-induced myocardial hypertrophy. *Am J Physiol Heart Circ Physiol* 315: H502–H511, 2018. doi:10.1152/ajpheart.00202.2018.
54. **Shapiro S**, **Traiger GL**, **Turner M**, **McGoon MD**, **Wason P**, **Barst RJ.** Sex differences in the diagnosis, treatment, and outcome of patients with pulmonary arterial hypertension enrolled in the registry to evaluate early and long-term pulmonary arterial hypertension disease management. *Chest* 141: 363–373, 2012. doi:10.1378/chest.10-3114.
55. **Skavdahl M**, **Steenbergen C**, **Clark J**, **Myers P**, **Demianenko T**, **Mao L**, **Rockman HA**, **Korach KS**, **Murphy E.** Estrogen receptor-beta mediates male-female differences in the development of pressure overload hypertrophy. *Am J Physiol Heart Circ Physiol* 288: H469–H476, 2005. doi:10.1152/ajpheart.00723.2004.
57. **Tetri LH**, **Diffee GM**, **Barton GP**, **Braun RK**, **Yoder HE**, **Haraldsdottir K**, **Eldridge MW**, **Goss KN.** Sex-specific skeletal muscle fatigability and decreased mitochondrial oxidative capacity in adult rats exposed to postnatal hyperoxia. *Front Physiol* 9: 326, 2018. doi:10.3389/fphys.2018.00326.
58. **Teyssier C**, **Belguise K**, **Galtier F**, **Chalbos D.** Characterization of the physical interaction between estrogen receptor alpha and JUN proteins. *J Biol Chem* 276: 36361–36369, 2001. doi:10.1074/jbc.M101806200.
59. **Trip P**, **Rain S**, **Handoko ML**, **van der Bruggen C**, **Bogaard HJ**, **Marcus JT**, **Boonstra A**, **Westerhof N**, **Vonk-Noordegraaf A**, **de Man FS.** Clinical relevance of right ventricular diastolic stiffness in pulmonary hypertension. *Eur Respir J* 45: 1603–1612, 2015. doi:10.1183/09031936.00156714.
61. **Umar S**, **Iorga A**, **Matori H**, **Nadadur RD**, **Li J**, **Maltese F**, **van der Laarse A**, **Eghbali M.** Estrogen rescues preexisting severe pulmonary hypertension in rats. *Am J Respir Crit Care Med* 184: 715–723, 2011. doi:10.1164/rccm.201101-0078OC.
63. **Vonk Noordegraaf A**, **Chin KM**, **Haddad F**, **Hassoun PM**, **Hemnes AR**, **Hopkins SR**, **Kawut SM**, **Langleben D**, **Lumens J**, **Naeije R.** Pathophysiology of the right ventricle and of the pulmonary circulation in pulmonary hypertension: an update. *Eur Respir J* 53: 1801900, 2019. doi:10.1183/13993003.01900-2018.
64. **Vonk Noordegraaf A**, **Westerhof BE**, **Westerhof N.** The relationship between the right ventricle and its load in pulmonary hypertension. *J Am Coll Cardiol* 69: 236–243, 2017. doi:10.1016/j.jacc.2016.10.047.
65. **Vonk-Noordegraaf A**, **Haddad F**, **Chin KM**, **Forfia PR**, **Kawut SM**, **Lumens J**, **Naeije R**, **Newman J**, **Oudiz RJ**, **Provencher S**, **Torbicki A**, **Voelkel NF**, **Hassoun PM.** Right heart adaptation to pulmonary arterial hypertension: physiology and pathobiology. *J Am Coll Cardiol* 62, *Suppl*: D22–D33, 2013. doi:10.1016/j.jacc.2013.10.027.

66. **Wang M**, **Crisostomo P**, **Wairiuko GM**, **Meldrum DR.** Estrogen receptor-alpha mediates acute myocardial protection in females. *Am J Physiol Heart Circ Physiol* 290: H2204–H2209, 2006. doi:10.1152/ajpheart.01219.2005.
67. **Wang Z**, **Patel JR**, **Schreier DA**, **Hacker TA**, **Moss RL**, **Chesler NC.** Organ-level right ventricular dysfunction with preserved Frank-Starling mechanism in a mouse model of pulmonary arterial hypertension. *J Appl Physiol (1985)* 124: 1244–1253, 2018. doi:10.1152/japplphysiol.00725.2017.
68. **Wei CC**, **Chen Y**, **Powell LC**, **Zheng J**, **Shi K**, **Bradley WE**, **Powell PC**, **Ahmad S**, **Ferrario CM**, **Dell'Italia LJ.** Cardiac kallikrein-kinin system is upregulated in chronic volume overload and mediates an inflammatory induced collagen loss. *PLoS One* 7: e40110, 2012. doi:10.1371/journal.pone.0040110.
69. **Weiss JL**, **Frederiksen JW**, **Weisfeldt ML.** Hemodynamic determinants of the time-course of fall in canine left ventricular pressure. *J Clin Invest* 58: 751–760, 1976. doi:10.1172/JCI108522.
70. **Windak R**, **Müller J**, **Felley A**, **Akhmedov A**, **Wagner EF**, **Pedrazzini T**, **Sumara G**, **Ricci R.** The AP-1 transcription factor c-Jun prevents stress-imposed maladaptive remodeling of the heart. *PLoS One* 8: e73294, 2013. doi:10.1371/journal.pone.0073294.
71. **Yalcinkaya E**, **Celik M**, **Bugan B.** Extracellular matrix turnover: a balance between MMPs and their inhibitors. *Arq Bras Cardiol* 102: 519–520, 2014. doi:10.5935/abc.20140061.
72. **Yarbrough WM**, **Baicu C**, **Mukherjee R**, **Van Laer A**, **Rivers WT**, **McKinney RA**, **Prescott CB**, **Stroud RE**, **Freels PD**, **Zellars KN**, **Zile MR**, **Spinale FG.** Cardiac-restricted overexpression or deletion of tissue inhibitor of matrix metalloproteinase-4: differential effects on left ventricular structure and function following pressure overload-induced hypertrophy. *Am J Physiol Heart Circ Physiol* 307: H752–H761, 2014. doi:10.1152/ajpheart.00063.2014.
73. **You J**, **Wu J**, **Zhang Q**, **Ye Y**, **Wang S**, **Huang J**, **Liu H**, **Wang X**, **Zhang W**, **Bu L**, **Li J**, **Lin L**, **Ge J**, **Zou Y.** Differential cardiac hypertrophy and signaling pathways in pressure versus volume overload. *Am J Physiol Heart Circ Physiol* 314: H552–H562, 2018.
74. **Zhai P**, **Eurell TE**, **Cooke PS**, **Lubahn DB**, **Gross DR.** Myocardial ischemia-reperfusion injury in estrogen receptor-alpha knockout and wild-type mice. *Am J Physiol Heart Circ Physiol* 278: H1640–H1647, 2000. doi:10.1152/ajpheart.2000.278.5.H1640.